arXiv:1610.09861v1 [physics.atom-ph] 31 Oct 2016

The D_1 enigma and its physical origin

J. O. Stenflo[1,2]
[1]*Institute for Astronomy, ETH Zurich, CH-8093 Zurich, Switzerland*
[2]*Istituto Ricerche Solari Locarno, Via Patocchi, 6605 Locarno-Monti, Switzerland*
stenflo@astro.phys.ethz.ch

Abstract

The D_1 enigma is an anomaly, which was first observed on the Sun as a symmetric polarization peak centered in the core of the sodium D_1 line that is expected to be intrinsically unpolarizable. To resolve this problem the underlying physics was later explored in the laboratory for D_1 scattering at potassium vapor. The experiment showed that the scattering phase matrix element P_{21} is positive while P_{22} is negative, although standard quantum scattering theory predicts that both should be zero. This experimental contradiction is currently the main manifestation of the D_1 enigma. Subsequent theoretical studies showed that such polarization effects may arise if scattering theory is extended to allow for interference effects due to level splittings of the ground state, in contrast to standard scattering theory, which only allows for interferences from level splittings of the intermediate state. Previous attempts to implement this idea had to rely on heuristic arguments to allow modeling of the experimental data. In the present paper we develop a formulation of the theory that can be self-consistently applied to quantum systems with any combination of electronic and nuclear spins. No statistical equilibrium or optical pumping is needed. The atom is assumed to be unpolarized at the beginning of each scattering event. The theory is capable of explaining both the phase matrix behavior of the laboratory data and the existence of a symmetric polarization peak in the core of the solar D_1 line. We also use it to predict the polarization structures that we expect to see in a next-generation laboratory experiment with the rubidium isotopes ^{87}Rb and ^{85}Rb.

Subject headings: polarization – scattering – techniques: spectroscopic – Sun: atmosphere – line: profiles – methods: laboratory: atomic

1. Introduction

It has been widely believed that such a fundamental physical process as the quantum scattering of visible light is well understood, because the theory was developed and tested already in the 1920s during the initial phase of the development of quantum mechanics. The experimental tests at that time were however crude in comparison with the possibilites offered by today's technology, and they were largely discontinued around 1935, when the focus of the physics community turned to other topics.

A renewed interest in the basic physics of polarized light scattering arose via solar physics through the discovery that the Sun's spectrum is richly structured in linear polarization by coherent scattering processes. This polarization, referred to as SS2 or the "Second Solar Spectrum" (cf. Stenflo & Keller 1996, 1997), is a scattering phenomenon that is not caused by external magnetic fields although it is modified by them through the Hanle effect. The wealth of unfamiliar and apparently anomalous polarization phenomena in SS2 led to the recognition of the need for deepened explorations of the theoretical foundations and for experimental tests of the theory with the precision that today's technology allows. The prime enigma that confronted the theory was the anomalous Na I D_1 5896 Å line, because standard quantum theory predicts that it should be nearly unpolarizable, in contradiction with the solar observations, which

revealed it to possess polarization structure.

The main question then was whether the D_1 enigma is a problem of solar physics or of quantum physics (or both). While considerable theoretical efforts have been invested in the modeling of the solar Na I D_1 line (e.g. Landi Degl'Innocenti 1998; Belluzzi et al. 2015), it was recognized that a laboratory experiment on polarized scattering under controlled conditions was required to obtain an unequivocal answer to the question whether there is something that has been overlooked in quantum scattering theory. The Sun's dynamic and stratified optically thick atmosphere with tangled magnetic fields and complicated geometry is a complex medium that is governed by many unknown parameters, which makes it unsuited as a laboratory for definite tests of fundamental physical theories. One needs to set up an experiment that cleanly isolates the physical processes to be explored, without confusion from irrelevant effects.

For this reason a laboratory experiment for polarized D_1 scattering under the simplest possible controlled conditions (single scattering at 90°) was carried out a decade ago to determine the elements of the Mueller scattering matrix and compare them with theoretical predictions, with the aim of either verifying or falsifying available scattering theory. The experiment revealed considerable polarization structure of the D_1 line where standard scattering theory predicts null results (Thalmann et al. 2006, 2009), which gave us an unequivocal answer to our basic question: The D_1 enigma is indeed a problem of quantum physics. Figure 1 illustrates the most relevant experimental results.

The unavoidable conclusion is that any scattering theory that is unable to confront and explain the laboratory data must be considered as incomplete. In the solar case the situation is more ambiguous, because the Na I D_1 polarization profile is observed to have a diversity of shapes and amplitudes. However, among these various D_1 signatures it is the existence of a symmetric D_1 polarization peak (Stenflo et al. 2000a,b) that has remained enigmatic from the point of view of quantum theory, and not so much the other more antisymmetric profiles.

In the search for explanations of the enigmatic laboratory data it was realized that if one would allow for interferences between pairs of scattering amplitudes for which the initial magnetic substates or the final substates of a given pair are not the same (such terms are prohibited in standard scattering theory), then the scattered radiation could acquire polarization of the observed kind (Stenflo 2009). These ideas were further developed and used for modeling of the experimental data in Stenflo (2015a,b).

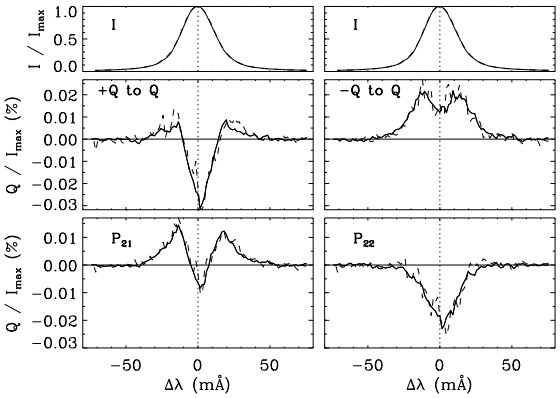

Fig. 1.— Laboratory results for scattering of linear polarization at potassium gas in the D_1 line at 7699 Å (adapted from Thalmann et al. 2006). The linear polarization of the incident radiation is either perpendiculat ($+Q$) or parallel ($-Q$) to the scattering plane, and Stokes Q is measured in the scattered radiation (middle panels, while the top panels give the scattered Stokes I or P_{11}). The phase matrix elements P_{21} and P_{22} in the bottom panels are obtained from the two middle panels as half the sum and half the difference. The circumstance that the solid lines, which represent the use of full laser power, are indistinguishable (within the noise fluctuations) from the dotted lines, which represent the case when the laser power has been reduced by a factor of 10, provides evidence that we are in the regime of linear optics. Available scattering theory predicts zero polarization for the middle and bottom panels and is therefore unequivocally contradicted by the experiment.

The difficulty was to show how these ideas could be implemented in a self-consistent way. The phenomenological treatments in Stenflo (2009, 2015a,b) contained heuristic arguments that could not be directly generalized for applications to arbitrary quantum systems. In the present paper we replace this approach with a more well defined and

consistent theoretical framework, which provides an explanation for both the laboratory results in Figure 1 and for the existence of a symmetric and positive polarization peak in the core of the solar Na D_1 line. No optical pumping or statistical equilibrium is used. The atom is assumed to be unpolarized at the beginning of any given scattering event. It is verified that the theory obeys the principle of spectroscopic stability (in the limit of vanishing fine and hyperfine structure splitting) for any combination of electronic and nuclear spins.

A common reaction to the previous attempts to modify quantum scattering theory has been one of disbelief, because quantum mechanics has already survived scrutiny and experimental tests for more than nine decades. This rejection is based on a misunderstanding. The modifications that have been proposed in the previous papers as well as in the present one do not change anything at all in the Schrödinger equation, in the way we calculate Feynman diagrams, or in the evolution of the wave function. The computation of scattering probability amplitudes is not being questioned. The problem lies exclusively in the procedure that we use to go from the unobservable probability amplitudes to observables (probabilities) in the case of multilevel atomic systems. This procedure is not governed by any Schrödinger equation or Feynman diagrams, and it has not been tested previously in the parameter domain that is relevant to D_1 scattering.

In a next-generation laboratory experiment we plan to test the theory with collision-free scattering at rubidium vapor. We therefore show in Section 7 the predicted linearly polarized D_1 profiles of the hyperfine structure components of the two main isotopes ^{87}Rb and ^{85}Rb. Like for scattering at sodium and potassium the tell-tale signature of the new scattering terms is that the D_1 phase matrix elements P_{21} and P_{22} are non-zero and of opposite signs. Without the new terms these matrix elements would be zero.

2. Use of laser radiation to explore polarized scattering in the weak radiation limit

Although the experimental falsification of standard scattering theory as expressed by Figure 1 is clear and unambiguous, it has been dismissed on the grounds that laser light is special (because of its coherent nature and high energy density) and cannot be used for testing how natural radiation is scattered by physical systems. Besides the remark that there cannot be anything wrong with quantum mechanics this has been the unsubstantiated justification for repeatedly rejecting papers on this topic.

Let us therefore here address in some detail the question whether the determination of the elements of the Mueller scattering matrix in any way depends on whether a laser or any other kind of lamp is used as a light source. There are two aspects of this: (i) the coherent nature of laser light, and (ii) the high energy density of the laser beam, which makes the medium non-linear. In Figure 1 the indistinguishability (within the noise fluctuations) of the solid and dashed curves, which represent recordings with full laser power (solid) and the power reduced by a factor of ten (dashed), constitutes experimental verification that there is no dependence of the scattering polarization on the intensity of the incident radiation. This implies that we are indeed in the regime of linear optics. We will return to the issue of the energy density later in this section, but with the experimental verification of no intensity dependence, which implies that our results are representative of the weak radiation limit, we next focus on the issue of the coherent nature of laser radiation.

As long as we are in the regime of linear optics, when the physical properties of the medium to be studied do not depend on the ambient radiation field, the polarizing properties of the medium are completely described by the 4×4 Mueller scattering matrix, which relates the incoming and outgoing Stokes vectors to each other. When dividing the matrix elements by the intensity to get the fractional polarizations, the Mueller matrix contains 15 independent elements. They are determined by sending in a sequence of light beams with known polarization states (100 % linear, circular, etc.) and then measuring the Stokes vector of the output beam. The medium can for instance be a weakly polarizing instrument, a polarization modulation system, or a gas that polarizes through light scattering. This medium can be considered as a "black box" with unknown physical properties that are the sources of the polarization effects.

The measuring procedure to determine the 15 independent Mueller matrix elements is independent of the internal physics of the black box.

The coherence depth of the photons of the light source used for this calibration of the Mueller matrix is irrelevant. If we determine the polarization properties of an optical system, the results are independent of the type of light source used, whether it is laser radiation or a broad-band lamp (combined with a narrow-band filter, if one wants good spectral selection). The only thing that matters is the polarization state of the incident radiation. Because of the coherent nature of laser light, it is naturally polarized, but by inserting known polarization filters in the incident beam, we always ensure that all the incident photons have identical polarization state, regardless of whether the photons originate from a laser or from a lamp.

Natural light (like solar radiation) is only partially polarized, because it consists of an ensemble of uncorrelated wave packets (photons). When doing the ensemble averaging (incoherent summation) one generally gets weak partial polarization, although each individual component of the ensemble may represent 100 % elliptical polarization. However, when letting natural (or laser) light pass through a polarizing filter, one ensures that the polarization state of all wave packets will be the same. The coherence length or relative phase correlations between the wave packets are irrelevant for the determination of the Mueller matrix, only the polarization state matters.

We are free to mathematically decompose any light beam (natural or laser) in its fundamental components, and then do ensemble averaging over the bilinear products of their respective amplitudes. These bilinear products represent contributions to the four Stokes parameters). The most natural mathematical decomposition is in terms of the Fourier components (plane waves, infinite sine or cosine waves) of the radiation field. We can then do the ensemble averaging over the bilinear products of these Fourier components. Nothing can be more coherent than a single Fourier component (since it has infinite coherence depth). Laser radiation may be thought of as an approximation of a single Fourier component per polarization state. The ensemble average is then particularly simple, but as mentioned before, this is irrelevant for our problem, because it is only the polarization state that matters, and the polarization filter ensures that all the components of the ensemble have identical polarization.

Let us now return to the often heard claim that laser radiation is different because of its high energy density. In intense laser beams, when the so-called Rabi frequency ω_R is much larger than the damping width, the atom gets "dressed" by the radiation field (cf. Cohen-Tannoudji & Reynaud 1977), which leads to frequency splitting and affects the positions, amplitudes, and widths of the components in the scattered spectrum. $\hbar\omega_R$ represents the interaction energy between the atom and the radiation field. The Rabi frequency depends on the radiation energy density of the beam in the vapor cell, which in turn depends on the laser power and the cross section of the expanded beam (in our case expanded to $1\,\mathrm{cm}^2$ to fill the scattering region of the vapor cell). In Appendix A we have computed the Rabi frequency for our experimental setup. When the laser is used with maximum power (15 mW) the Rabi frequency is 2.1 times the radiative damping width, or 0.25 mÅ in wavelength units. This is well below the laser band width and about 38 times smaller than the collisionally enlarged damping width. We are not aware of any theoretical demonstration that this rather small value of the Rabi frequency would cause any observable polarization effects (and we note that the level splitting, being smaller than the laser band width, is not observable).

Still, the only conclusive way to rule out any possible non-linear effects due to the energy density of the laser beam is to do it experimentally. We have done the scattering measurements both with full laser power and with the power reduced by a factor of ten. The results are found to be identical within the noise fluctuations, as we have seen in Figure 1. This verifies that there is indeed no dependence on the laser intensity over the covered range. This in turn implies that the results are also valid in the weak radiation limit.

Doubters may argue that our factor of ten range does not warrant extrapolation to the weak radiation limit. However, from the constancy over a factor of 10 we have absolutely no reason to expect that anything would change if we would further lower the laser power by a factor of 100 or 1000. In principle such confirmation could be carried out (and anyone who feels that it would be important

could do this), but since the noise level goes up when reducing the laser power, one would need to compensate with prolonged integration times, until these times get prohibitively long. For the time being the verification of the regime of linear optics over the factor of 10 is for all practical purposes good enough to allow us to proceed with the quantitative modeling of the experiment on the assumption that we are indeed in the regime of linear optics.

2.1. Early attempts with ordinary lamps as light source

It has repeatedly been argued that it would be better to use a normal laboratory lamp as a light source for a scattering experiment. As a matter of fact this is what we did when we began to develop the experiment more than a decade ago, but this approach failed for two reasons: (1) The achievable S/N ratio was much too small for detection of the subtle polarization effects in the D_1 line, and (2) it was not possible to sufficiently isolate D_1 from possible contaminations caused by D_2. Also it was not feasible to spectrally resolve the various components of the quantum system under study.

Our first attempt was with a vapor cell for the yellow sodium lines, a broad-band lamp as light source, and a Lyot element to discriminate between the contributions from D_1 and D_2. This approach failed because of insufficient discrimination blocking ratio due to the finite acceptance angle of the Lyot element, in combination with the wide solid angle of the scattered beam (needed to collect sufficient photons). In addition the S/N ratio was insufficient to reveal the subtle polarization effects in the D_1 line.

We also considered spectral selection in the scattered beam. A spectrograph solution can be ruled out because of vastly insufficient optical throughput through its narrow entrance slit. One instead needs a wide-angle narrow-band filter system. This insight led us to acquire two tunable, lithium-niobate Fabry-Perot etalons that we could use in dual configuration to suppress side lobes and ghosts. Still this approach was found to be both cumbersome and not successful enough, because the ghost suppression was generally insufficient to achieve the needed discrimination ratio with respect to D_2. All this is documented in the excellent PhD thesis of Feller (2008). It represents a development phase that now is far behind us, and which led us to the insight that a successful D_1 polarization experiment could only be done with a tunable laser, to get the needed S/N ratio and spectral resolution. It was always clear that one then needs to experimentally verify that we are in the regime of linear optics, and that when this condition is satisfied the coherent nature of laser radiation will not be an issue for the determination of the polarization properties of the potassium gas.

3. Coherency matrix formulation

The theoretical framework that has been developed in the monumental monograph by Landi Degl'Innocenti & Landolfi (2004) is based on the flat-spectrum approximation (cf. p. 257 of that monograph). This approximation requires that the incident radiation is broad-band, which implies that the incoming wave packets have vanishing coherence depth. In contrast, we know that actual natural light consists of wave packets with a coherence depths of several meters, the distance that light travels during the time $1/\gamma$, where γ is the damping constant (cf. Stenflo 2011).

It is a fundamental principle of quantum physics that any radiation field (laser or natural light) can be described in terms of a linear superposition of its Fourier components (or plane waves). We need a scattering theory that allows us to compute the scattering probability amplitude separately for each individual Fourier component (each of which has infinite coherence depth). This is possible in the framework of the Kramers-Heisenberg scattering formalism, but it is prohibited by the flat-spectrum approximation.

The Kramers-Heisenberg (K-H) dispersion formula for radiative scattering was introduced in the early days of quantum mechanics (Kramers & Heisenberg 1925), but Dirac (1947) later presented it in the notational form that we generally use today. The K-H scattering probability amplitude is the sum of two terms, one resonant term representing absorption followed by emission, and one non-resonant term representing emission followed by absorption. Here we can safely make the so-called rotating-wave approximation and ignore the non-resonant term, since it is vanishingly small in comparison with the resonant one unless we are very far from the resonance. The K-H probability amplitude for

scattering $a \rightarrow b \rightarrow f$ is then

$$w_{\alpha\beta} \sim \langle\, f \,|\, \hat{\boldsymbol{r}} \cdot \boldsymbol{e}_\alpha \,|\, b \,\rangle \, \langle\, b \,|\, \hat{\boldsymbol{r}} \cdot \boldsymbol{e}_\beta \,|\, a \,\rangle \, \Phi_{ba} \qquad (1)$$

(cf. Stenflo 1994, 1998). Here

$$\Phi_{ba} = \frac{2/i}{\omega_{ba} - \omega' - i\gamma/2}\,, \qquad (2)$$

where ω' is the frequency of the incident radiation, while

$$\omega_{ba} = (E_b - E_a)/\hbar \qquad (3)$$

is the transition frequency between the energy levels of the upper and lower magnetic substates b and a. Indices α and β refer to the polarization states of the emitted and incident radiation, respectively.

Symbol $w_{\alpha\beta}$ represents the elements of a complex 2×2 matrix $\boldsymbol{w}$. The way in which these elements are being calculated is not questioned here. To go from these probability amplitudes, which are unobservable, to probabilities that represent observable quantities, we need to do ensemble averaging over the bilinear products $w_{\alpha\beta}\, w^*_{\alpha'\beta'}$. They represent components of the 4×4 coherency matrix $\boldsymbol{W}$ that is constructed from the $\boldsymbol{w}$ amplitude matrices via a tensor product:

$$\boldsymbol{W} \;=\; \Big(\sum_{abf} \boldsymbol{w}\Big) \otimes \Big(\sum_{a'b'f'} \boldsymbol{w}^*\Big)\,(\,\mathscr{S}_{\rm standard} + \mathscr{S}_{\rm new}). \qquad (4)$$

This is an unfamiliar way of expressing $\boldsymbol{W}$, because we have introduced a separate bracket with the two $\mathscr{S}$ terms, which have the purpose of explicitly defining how the a, b, f states should be combined with the a', b', f' states. Far from all combinations are allowed. The problem that we are addressing here is how to correctly determine which combinations should be allowed, and which should be prohibited.

The standard way of writing $\boldsymbol{W}$ is without these $\mathscr{S}$ terms, while breaking up the summations into two categories: the summations over the intermediate states b and b', which are done coherently (separately for $\boldsymbol{w}$ and $\boldsymbol{w}^*$), and the summations over the initial and final states a and f, which are done incoherently (over the tensor products, not over the amplitudes, with the condition that $a = a'$ and $f = f'$). The scattering process takes us from a definite initial to a definite final state via all possible intermediate states. With this prescription the only interference terms that are allowed are between scattering amplitudes that refer to different intermediate states b and b'. Interferences between scattering amplitudes for which $a \neq a'$ or $f \neq f'$ are prohibited.

According to the way in which Equation (4) has been expressed, all summations are formally allowed to be coherent in the first two brackets. The mentioned restriction that the initial and final states should be summed over incoherently is enforced by the selection term $\mathscr{S}_{\rm standard}$. It can be expressed as the product of two Kronecker deltas, which implement the selection rule $a = a'$ and $f = f'$:

$$\mathscr{S}_{\rm standard} = \delta_{aa'}\, \delta_{ff'}\,. \qquad (5)$$

In the present paper we will argue that the standard scattering scenario that is defined by Equation (5) is too restrictive and blocks the occurrence of valid interference terms that significantly affect the scattering polarization that we can observe in the laboratory and on the Sun. These previously overlooked terms can be formally unblocked by adding the new "selection term" $\mathscr{S}_{\rm new}$ in Equation (4). In Section 4 we address the problem how to identify the missing terms and define the expression for $\mathscr{S}_{\rm new}$ in a way that is unambiguous and physically self-consistent for any quantum system with any combination of electronic and nuclear spins. As a preparation and for conceptual guidance we discuss in the next subsection how we can think about the nature of the radiation-matter interaction process in the case of a multilevel atomic system, and about the role of the tensor components of the electric dipole moment.

3.1. The resonant tensor components of the electric dipole moment

The expression of Equation (1) for the K-H scattering amplitude contains two matrix elements, one for the absorption and one for the emission leg of the scattering transition. Conceptually each matrix element, e.g. the one that connects levels b and a, can be thought of as a resonant "string", in this example with resonant frequency ω_{ba} and "string ends" at states $|\, b\rangle$ and $|a\rangle$. The string oscillations are excited by the electric field - dipole interaction $\boldsymbol{d} \cdot \boldsymbol{E}'$, where $\boldsymbol{d} = -e\boldsymbol{r}$ is the electric dipole moment, and $\boldsymbol{E}'$ is the os-

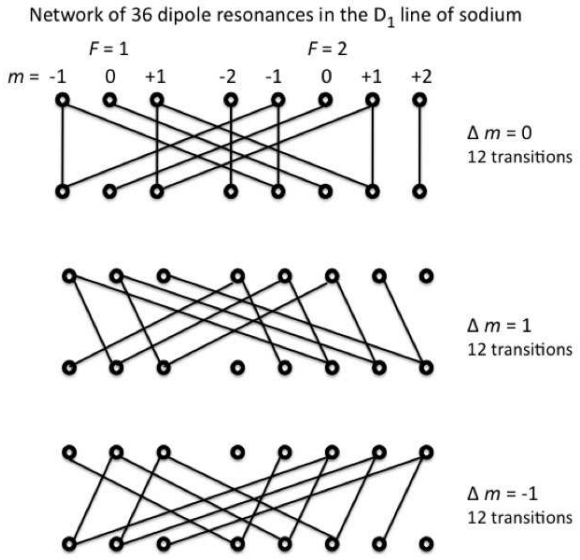
Network of 36 dipole resonances in the D1 line of sodium
F = 1
F = 2
m = -1 0 +1 -2 -1 0 +1 +2
Δ m = 0
12 transitions
Δ m = 1
12 transitions
Δ m = -1
12 transitions

Fig. 2.— Illustration of the 36 resonances of the sodium D_1 line transition that are collectively excited by the driving incident radiation field. Each resonance represents a tensor component of the electric dipole moment of the atomic system.

cillating electric vector of the incident radiation field. For a $J = 0 \rightarrow 1$ absorption transition we only sum over three "strings", which represent the three spatial components of $\boldsymbol{d}$. In this particular case $\boldsymbol{d}$ can be treated as a vector. In the general case, however, the dipole moment is a tensor, because the components have two indices (representing the two "end points"), and each such tensor component represents a resonant string.

Figure 2 illustrates that even for the relatively simple case of the D_1 line of sodium the number of resonances or "strings" that collectively make up this $J = 1/2 \rightarrow 1/2$ transition is quite large, namely 36. Potassium, barium, and lithium all have a D_1 line with exactly the same resonance structure (although with different resonance frequencies). All these chemical elements have nuclear spin 3/2, which induces a split of both the lower and upper $J = 1/2$ states into hyperfine structure states with total angular momentum quantum numbers $F = 1$ and 2. Since each F state has $2F + 1$ magnetic substates, there are 8 substates each in the lower and upper levels. The number of allowed electric dipole resonant transitions that connect them is 12 each for transitions with $q = \Delta m = 0, \pm 1$, which makes a total of 36 resonances.

The electric-field component E'_q of the incident radiation simultaneously drives the 12 oscillators with $m_a - m_b = q$. In general the incident radiation field has contributions from all three q values of E'_q. Then the radiation field drives oscillations of all the 36 "strings". We focus our discussion here on the D_1 line, because standard quantum scattering theory predicts it to be a polarization "null line", in unequivocal contradiction with experimental data.

3.2. Induced phase-locking between the scattering amplitudes

In general all 36 resonators get driven by the oscillations of the incident elctric field, and all these oscillators interfere with each other as expressed by the tensor product in Equation (4). However, unless the initially random phases between a given pair of oscillators get phase-locked by the incident radiation, the corresponding interference term vanishes when we do ensemble averaging.

In standard scattering theory there is an indirect way that has been used to allow for initial-state coherences, namely through preconditioning of the atomic system by optical pumping that takes place prior to the examined scattering event. Equation (4) can be generalized to include this possibility, by attaching the lower level amplitude factors, c_a attached to $\boldsymbol{w}$, and $c^*_{a'}$ attached to $\boldsymbol{w}^*$. The preconditioning process has to include phase synchronization between the respective sublevels, otherwise the off-diagonal terms of the lower-state density matrix (that represents ensemble averages over $c_a c^*_{a'}$) would be zero. The conclusion has been that if all off-diagonal terms of the ground-state atomic density matrix are zero (at the beginning of the scattering event), then there will be no contributions from scattering transitions with $a \neq a'$, which leads to the restriction that is expressed by Equation (5).

The physics that we deal with here is very different. No optical pumping is involved, and there is no reference to any c_a amplitude factors. They are not needed for the same kind of reason that amplitude factors c_b and $c_{b'}$ are not needed when we consider interference between the intermediate states b and b' in the sum over histories scenario.

At the beginning of the scattering event the off-diagonal elements of the excited atomic state are zero (in the absence of preconditioning by optical pumping). The phase synchronization between states b and b' that is a requirement for interference effects is accomplished by the driving electromagnetic field of the incident radiation. Similarly, the incident radiation is capable of synchronizing the relative phases of initial states a and a'. Also this synchronization is done without the need for any optical pumping or preconditioning of the atomic density matrix elements. In our present treatment the atomic system is instead assumed to be unpolarized at the beginning of each given scattering event, i.e., all off-diagonal density matrix elements are assumed to be zero.

There is an additional reason why the atomic amplitude factors c_a and $c_{a'}$ or the corresponding density matrix elements should not appear in our expression for the coherency matrix. Their presence would in general imply that the coherency matrix (and therefore also the Mueller scattering matrix) is not just a function of the properties of the material medium but also of the ambient radiation field (its intensity, in combination with its polarization state and directional properties). This means that we would be in the regime of nonlinear optics. Here our aim is to formulate a theory that is representative of the weak radiation limit of linear optics, and our experimental tests with varying laser power verify that the experiment indeed deals with that regime. With no reference to the atomic amplitude factors in the expression of Equation (4) for the coherency matrix we achieve that the scattering matrix is expressed in a way that is manifestly independent of the ambient radiation field, and that it therefore represents the regime of linear optics.

4. Procedure to identify the new interference terms in an unambiguous way

The tensor product in Equation (4) allows for a large number of bilinear products between scattering probabilities, each of which could potentially be a source of observable interference effects, provided that they survive ensemble averaging. The restriction that defines the subset of cross terms, which correspond to physically valid interference terms, is represented by the selection factor $\mathscr{S}$. The mathematical expression for this factor has to be physically consistent for any quantum system. This consistency requirement can be exploited to eliminate ambiguities in the determination of $\mathscr{S}$ and can be expressed in terms of two constraints that we will apply: (i) The Principle of Spectroscopic Stability, and (ii) the condition for phase-locking by the radiation field. Next we will elaborate on these two constraints and arrive at a unique expression for $\mathscr{S}_{\text{new}}$.

4.1. Principle of spectroscopic stability as a selection criterion

In the absence of electron spin S and nuclear spin I ground states cannot be split or be polarized, and the scattering transition is of the "classical" type $L = 0 \rightarrow 1 \rightarrow 0$. In the presence of fine structure or hyperfine structure splitting, we get scattering contributions from many more combinations of magnetic substates, as indicated by Equation (4) and Figure 2, with the potential for non-trivial selection terms $\mathscr{S}$. A necessary (although not sufficient) requirement is then that such terms must obey the Principle of Spectroscopic Stability (PSS).

The introduction of non-zero electronic and nuclear spins leads to multiple, split atomic levels, and the various transition amplitudes between the different levels get governed by complicated algebraic expressions that depend on the new quantum numbers. All these expressions contribute (with magnitude and sign) in an intricate way when summing over the various scattering histories in Equation (4) to compute the resulting scattering matrix. PSS in this context means that if we let the splitting (both fine and hyperfine) go to zero, such that the profile functions Φ_{ba}, which are part of the amplitudes $w_{\alpha\beta}$, will become identical for all the transitions, while doing the full calculation of the coherency matrix $\boldsymbol{W}$ with all the algebraic expressions for all the allowed scattering transitions between the combinations of fine and hyperfine structure states, then the resulting scattering matrix should be identical to the classical one for an $L = 0 \rightarrow 1 \rightarrow 0$ scattering transition. Letting the splitting go to zero while retaining the non-zero values of spins S and I is physically equivalent to replacing S and I by zero. While it is clear that such a PSS must be obeyed to preserve physical consistency, it looks like an "algebraic mira-

cle" that it is also satisfied mathematically, due to the apparent algebraic complexity of the expressions over which we sum. The algebraic expression for the dipole transition amplitude between two m states is given in Appendix B.

Note that the selection term $\mathscr{S}$ in Equation (4) has to obey the PSS criterion for all possible combinations of electronic and nuclear spins S and I. For instance, in the case of a D_1 type transition $S = 0.5$ while $I = 1.5$. There are a number of reasonable $\mathscr{S}$ term choices that satisfy PSS for this particular combination of S and I, but most of them fail to satisfy PSS for certain other combinations. Such choices must be rejected, because consistency requires that PSS must be satisfied for all possible S and I combinations. This criterion allows us to unambiguously weed out invalid choices. The "weeding" has been done with a computer program that loops through the various combinations of electronic and nuclear spins to verify that the properties of the $L = 0 \rightarrow 1 \rightarrow 0$ scattering matrix are retrieved in the zero-splitting limit for all quantum-number combinations.

In practice this is done by calculating the intrinsic polarizability W_2 and requiring that for vanishing splitting it must become unity, which is its classical dipole-scattering value. W_2 represents the fraction of scattering processes that behave like classical, Rayleigh-type dipole scattering, while the remaining fraction, $1 - W_2$, behaves like isotropic, unpolarized scattering. More explicitly, the Mueller scattering matrix (also referred to as the phase matrix), which describes how the Stokes vector is scattered, and which is constructed from the coherency matrix $\boldsymbol{W}$ via a purely mathematical transformation, can be written as (cf. Stenflo 1994)

$$\boldsymbol{P} = W_2 \boldsymbol{P}_R + (1 - W_2)\boldsymbol{E}_{11} + W_1 \boldsymbol{E}_{44} \tfrac{3}{2} \cos\phi\,, \quad (6)$$

where

$$\boldsymbol{P}_R = \frac{3}{4} \begin{pmatrix} 1 + \cos^2\phi & \sin^2\phi & 0 & 0 \\ \sin^2\phi & 1 + \cos^2\phi & 0 & 0 \\ 0 & 0 & 2\cos\phi & 0 \\ 0 & 0 & 0 & 0 \end{pmatrix} \quad (7)$$

is the classical Rayleigh phase matrix, ϕ is the scattering angle, $\boldsymbol{E_{ii}}$ is a 4×4 matrix with all elements zero except for position ii, where it becomes unity, and W_1 is an intrinsic polarizability coefficient that only relates to the circular polarization.

For any given fine-structure component, W_2 depends on the combination of J quantum numbers of the scattering transition. Let us take the example of D_2 and D_1 when the nuclear spin in neglected. Then the D_2 $J = 0.5 \rightarrow 1.5 \rightarrow 0.5$ transition has $W_2 = 0.5$, while the D_1 $J = 0.5 \rightarrow 0.5 \rightarrow 0.5$ transition has $W_2 = 0$. However, if one lets the fine-structure splitting go to zero, so that the transition amplitude profiles of the two lines superpose coherently, then W_2 becomes unity, as required by PSS.

Using Equations (6) and (7) we can express W_2 in terms of the matrix elements P_{ij} in a way that is independent of the scattering angle ϕ, as follows:

$$W_2 = \frac{2\,(P_{12} + P_{22})}{3\,P_{11} + 2\,P_{12} - P_{22}}\,. \quad (8)$$

In our computer application of the PSS criterion we calculate W_2 according to Equation (8) from the phase matrix derived for a given combination of electronic and nuclear spins, to check whether it satisfies the requirement of being unity for all combinations of quantum numbers.

4.2. Requirement of phase locking as a selection criterion

As explained in Section 3.1, the dipole transitions that connect an upper and a lower m state may be thought of as resonant strings with two ends, one in each connected m state. The string oscillations are driven by the radiation field. When forming the coherency matrix $\boldsymbol{W}$ in Equation (4) we get products between pairs of oscillators. These products will not survive ensemble averaging if the relative phases of the two oscillators are random. If however the two strings have one common end point, then the oscillations will get synchronized by the radiation field. If on the other hand neither the upper nor the lower pair of end points coincide for a given pair of strings, then the relative phase is random and the ensemble average vanishes. This random phase relation follows from our assumption that there is no atomic polarization at the start of the interaction with the radiation field, which implies that states a and a' are uncorrelated when they refer to different m states.

In standard scattering theory each string pair has common lower ends ($a = a'$ and $f = f'$), while the upper ends may differ, as expressed by the selection term $\mathscr{S}_{\rm standard}$ in Equation (5). It is readily

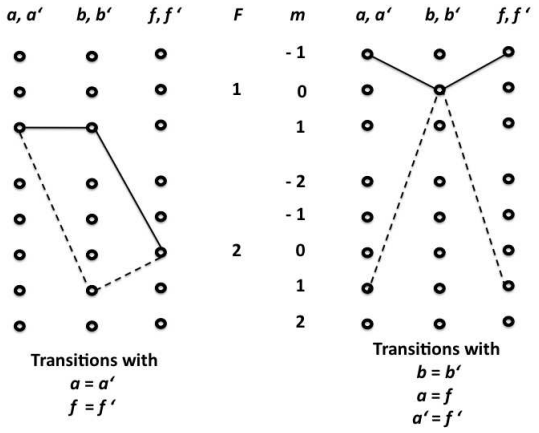

Fig. 3.— Illustration of D_1 scattering terms in the coherency matrix $\boldsymbol{W}$. The solid lines represent the amplitudes $\boldsymbol{w}$ for scattering $a \to b \to f$, while the dashed lines represent the amplitudes $\boldsymbol{w}^*$ for scattering $a' \to b' \to f'$. The D_1 transition has 8 lower and 8 upper m states, which may be connected by the scattering process. The left part of the figure illustrates the types of terms that are allowed in standard scattering theory, as defined by parameter $\mathscr{S}_{\rm standard}$ in Equation (5), while the right part of the figure illustrates the types of new terms that are governed by parameter $\mathscr{S}_{\rm new}$ in Equation (9).

verified that this term obeys PSS for all combinations of electronic and nuclear spins.

This is however not the only way to enable phase locking by the radiation field. It would become possible if we tie together the upper end points instead of the lower string end points. This implies that the new selection term $\mathscr{S}_{\rm new}$ should enforce $b = b'$ and therefore contain the factor $\delta_{bb'}$. In addition we need to have either $a \neq a'$ or $f \neq f'$ or both, because the special case when all a, b, and f ends are tied together is already included as a special case of $\mathscr{S}_{\rm standard}$. Therefore $\mathscr{S}_{\rm new}$ must also contain either the factor $1 - \delta_{aa'}$ or $1 - \delta_{ff'}$ or both.

4.3. Using the combined constraints to obtain a unique expression for $\mathscr{S}_{\rm new}$

When testing the different versions of $\mathscr{S}_{\rm new}$ that satisfy these phase-locking requirements we find that only two versions also satisfy PSS, and that only the following one of these two is also compatible with observations:

$$\mathscr{S}_{\rm new} = (1 - \delta_{aa'})\,(1 - \delta_{ff'})\,\delta_{b\,b'}\,\delta_{af}\;\delta_{a'f'}\,. \quad (9)$$

Note that in this expression we have left out a decoherence factor, which appears when the level splitting is non-zero. The origin of this decoherence factor will be dealt with in the next subsection.

First we recognize that the needed essential property of this version of $\mathscr{S}_{\rm new}$ is that it contains the factors δ_{af} and $\delta_{a'f'}$ which enforce that the initial and final m states are the same for each scattering amplitude of an interfering pair, as illustrated more explicitly in the right portion of Figure 3. This requirement makes the scattering process behave mathematically as if it would go from initial state b back to the same state via the intermediate states a and a', although in the physical reality it is a and a' that are the initial states.

The other version that also satisfies PSS is not unreasonable but a bit contrived. It is obtained if $\delta_{af}\delta_{a'f'}$ in Equation (9) is replaced by $\delta_{m_a m_f}\delta_{m_{a'} m_{f'}}$, i.e., the initial and final m states are enforced to be identical for each given scattering amplitude, while the initial and final F states are allowed to differ. However, this version has to be rejected because it leads to polarization effects that are not compatible with observations, in particular with those from the laboratory experiment on K D_1 scattering. This leaves us with Equation (9) as the only remaining physically consistent choice.

4.4. Applying the $\mathscr{S}_{\rm new}$ selection to split multiplets

Having settled for this definite choice of selection factor $\mathscr{S}$, which uniquely defines the subset of bilinear products that contribute to the coherency matrix $\boldsymbol{W}$ in the limit of vanishing splitting, let us next turn to the general case when the fine or hyperfine structure splitting is non-zero. Our task is to define how the interference and decoherence effects depend on the non-zero splitting.

For both the standard and new terms interference originates from the cross products $\Phi_{ba}\Phi^*_{b'a'}$ that appear when we form the bilinear products between scattering amplitudes $\boldsymbol{w}$ and $\boldsymbol{w}^*$ in the expression for the coherency matrix $\boldsymbol{W}$ (cf. Equations (1)–(4)). The decoherence effects can be factorized out from the frequency-dependent part by

converting the profile product to a profile sum (cf. Stenflo 1994):

$$\Phi_{ba}\Phi^*_{b'a'} \sim \cos\beta\; e^{i\beta}\; \tfrac{1}{2}(\Phi_{ba} + \Phi^*_{b'a'})\,, \qquad (10)$$

where

$$\tan\beta = \frac{\omega_{b'a'} - \omega_{ba}}{\gamma}\,, \qquad (11)$$

and γ is the damping constant. The factor $\frac{1}{2}$ is introduced to make the wavelength-dependent part of this expression area normalized. The decoherence is described by $\cos\beta\; e^{i\beta}$. When angle $\beta = 0$, the wavelength integration over the right-hand side gives unity.

When the interference involves only states with different m quantum numbers (for given J and F numbers), the decoherence is an expression of the Hanle effect, and angle β is referred to as the "Hanle angle". Since our treatment is much more general and includes interferences between states with any combination of quantum numbers (differing in m, J, or F or all of them at the same time), we will use the more general term "decoherence angle" for β.

In standard scattering theory $a = a'$, so that $\tan\beta = \omega_{b'b}/\gamma$. Then all decoherence effects are caused by splitting of the intermediate, excited state. For the new terms that are defined by $\mathscr{S}_{\rm new}$ we instead have $b = b'$, and then interference only happens because $a \neq a'$. In this case the decoherence angle is determined by

$$\tan\beta_g = \frac{\omega_{aa'}}{\gamma}\,, \qquad (12)$$

where $\omega_{aa'} = (E_a - E_{a'})/\hbar$ according to Equation (3). For clarity we have here introduced subscript g to mark that the decoherence is caused by the ground-state splitting.

In contrast to standard scattering theory the new terms need an additional decoherence factor, which we here refer to as $k_{\rm decoh}$ to distinguish it from the rest. It originates from a beat frequency between two separated intermediate metalevels within the excited state b. Let us explain. For simplicity we assume that the ground state has an infinite life time, which implies that the substates a and a' are infinitely sharp. If the incident radiation has frequency ω', then the radiatively excited metalevel, which belongs to level b, will have an energy that is $E_a + \hbar\,\omega'$ in the case of the scattering amplitude $\boldsymbol{w}$, while the intermediate metalevel for the $\boldsymbol{w}^*$ scattering amplitude will have the different energy $E_{a'} + \hbar\,\omega'$.

The energy difference between the two metalevels gives rise to beat oscillations, which are exponentially damped (with damping constant γ) because the excited state b has a limited life time. When doing ensemble averaging (in this case in the form of temporal integration over the damped oscillations) we get the decoherence factor

$$k_{\rm decoh} = \cos\beta_g\, e^{i\,\beta_g}\,, \qquad (13)$$

which is identical to the one obtained from the product of the profile functions and is also governed by Equation (12). Combining the two factors the total decoherence is found to be $\cos^2\beta_g\, e^{2i\,\beta_g}$.

The appearance of two decoherence factors that may be combined this way is familiar to us from PRD (partial frequency redistribution) theory: For the frequency coherent term $R_{\rm II}$ decoherence only appears once, due to the profile products of the absorption legs, while for the CRD term $R_{\rm III}$ there is an additional factor from the emission process. The origin of the second decoherence factor is however different in our case. Since we are here only dealing with the collision-free case, the scattering process is frequency coherent ($R_{\rm II}$ only) because of energy conservation. To understand that there is no contradiction it may be conceptually helpful to think of $k_{\rm decoh}$ as a branching ratio, because the beat oscillations, which cause it, effectively reduce the life time of the excited state.

The reason why there is no corresponding decoherence factor for "standard" scattering as represented by $\mathscr{S}_{\rm standard}$ is that the energies of the intermediate metalevels of the two scattering amplitudes are identical, thus without any beat oscillations. Since in "standard" theory $a' = a$, and level a is assumed to be infinitely sharp, the intermediate metalevel has energy $E_a + \hbar\,\omega'$ for both scattering amplitudes.

All our discussions that have led to the identification of the new interference terms and to their decoherence behavior may be expressed in final form in terms of our selection factor $\mathscr{S} =$

$\mathscr{S}_{\rm standard} + \mathscr{S}_{\rm new}$ as follows:

$$\mathscr{S} = \delta_{aa'}\,\delta_{ff'} + k_{\rm decoh}\,(1-\delta_{aa'})\,(1-\delta_{ff'})\,\delta_{b\,b'}\;\delta_{af}\;\delta_{a'f'}\,. \quad (14)$$

Note that we have here attached the extra decoherence factor $k_{\rm decoh}$ to the second term on the right-hand side. For the first term that represents standard theory this factor is unity and therefore does not appear, for the reasons that we have just explained. When this expression for $\mathscr{S}$ is used in Equation (4), the bilinear products between the profile factors Φ_{ba} automatically take care of the remaining decoherence effects for both the standard and new terms.

Let us finally make some clarifying remarks concerning the physical origin of the damping constant γ, which governs the magnitude of the interference and decoherence effects for the new terms of the extended theory. In previous papers we have referred to the new effects as due to ground-state coherences, but we now feel that such a terminology is misleading and should be abandoned, because it incorrectly suggests that the ground states have finite energy widths that cause them to partially overlap, and that this is the origin of the coherence effects. However, in our treatment we assume that the ground states have infinite life time and are therefore infinitely sharp. This implies that there is no partial overlap between their energy levels. The damping that is the cause of the partial overlap, decoherence effects, and interferences between the scattering amplitudes has its origin exclusively in the excited, intermediate state, both for the standard and the new scattering terms. Although the new interference effects are governed by the splitting of the infinitely narrow ground states, the damping that determines the magnitude of the effects comes from the excited state.

4.5. Implications for the scattering matrix

Applying our extended theory as defined by Equation (14) we show in Figure 4 the wavelength variation of the intrinsic polarizability W_2 across the Na D_2 and D_1 line system. Here W_2 has been derived from the phase matrix elements through Equation (8). We find that we get the identical W_2 function (the solid curve) with and without the $\mathscr{S}_{\rm new}$ term in Equation (4). The new interference effects thus do not affect W_2 for the D_2 – D_1 system.

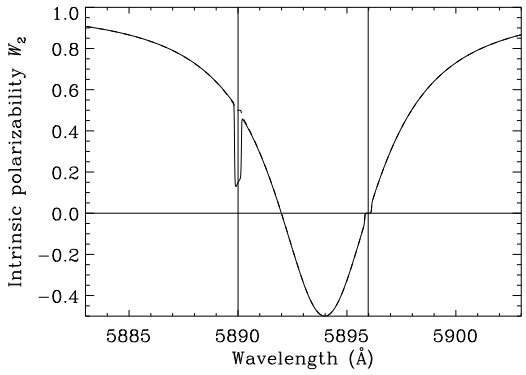

Fig. 4.— Intrinsic polarizability W_2 for the Na D_2 and D_1 line system as computed from the scattering matrix elements via Equation (8). The W_2 curve obtained with the new theory as defined by Equation (14) is identical to the one obtained with standard theory. The trough around the D_2 resonance is caused by the hyperfine structure splitting. When this splitting is neglected, we get the dashed curve, which differs from the solid one only through the absence of a D_2 trough.

The trough-like depression of W_2 around the D_2 resonance is induced by the hyperfine structure splitting. When we remove this splitting, i.e., set $I = 0$, we obtain the dashed curve in Figure 4, which coincides with the solid curve everywhere except in the Doppler core of the D_2 line, where the W_2 trough disappears and $W_2 = 0.5$. In the Doppler core of the D_1 line we always get $W_2 = 0$.

Note in Figure 4 that the W_2 curve asymptotically approaches unity in the far line wings. When we get far from the resonances in comparison with the magnitude of the fine-structure splitting, then the effects of the splitting become small and the scattering behavior approaches that of a classical dipole.

The new interferences instead manifest themselves in the form of a symmetry breaking between the P_{21} and P_{22} components of the phase matrix $\boldsymbol{P}$, as illustrated in Figure 5 for the 90° scattering case. We have plotted these components in normalized fractional polarization form, P_{21}/P_{11} as the solid line, and P_{22}/P_{11} as the dashed line. In

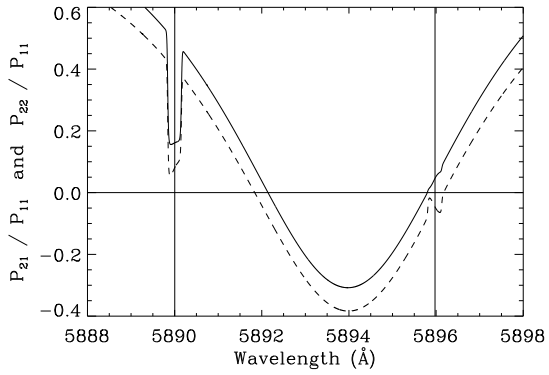

Fig. 5.— Symmetry breaking in the scattering matrix, illustrated for the 90° scattering case. The solid curve represents the fractional polarization P_{21}/P_{11}, which is the linear polarization that one would get when the incident radiation is unpolarized. For comparison, the dashed curve represents the ratio P_{22}/P_{11}. While P_{21} and P_{22} are the same in the standard theory, the new interference terms break this symmetry and cause the split between the solid and dashed curves. Notice in particular that at the D_1 resonance P_{21} is positive, while P_{22} is negative by the same amount.

standard scattering theory the solid and dashed lines would coincide and go through zero at the D_1 resonance. The systematic difference between them is exclusively caused by the new interferences.

Note that the relative shift between the curves is such that at the D_1 resonance P_{21}/P_{11} is significantly positive, while P_{22}/P_{11} is negative by the same amount, in qualitative agreement with the laboratory results for scattering in the potassium D_1 line that were illustrated in Figure 1. In Section 6 we will apply our new theory to model the laboratory measurements in considerable quantitative detail. First we will however apply the theory to explain the enigmatic existence of a symmetric polarization peak centered in the core of the solar Na D_1 line.

5. Solar polarization of the Na I D_1 and D_2 line system

Near (but inside) the solar limb the scattering geometry resembles that of 90° scattering, although the origin of the scattering polarization is the small anisotropy of the incident radiation field that manifests itself as the limb darkening of the solar disk. In good approximation while avoiding detailed angular integrations, one can think of the anisotropic radiation field as consisting of two components, one directional component that is the source of the polarization, and one isotropic component that dilutes the polarized radiation with unpolarized light. This dilution factor enters as a global scaling factor if we ignore the wavelength dependence of the anisotropy across the considered spectral window.

For exploratory, initial modeling of polarized line profiles before going into the technical complexities of polarized radiative transfer with partial frequency redistribution, it has often been found very useful to apply the Last Scattering Approximation (LSA, cf. Stenflo 1980, 1994). In the LSA scenario the last scattering event occurs at a particle that is illuminated by unpolarized incident radiation. The fractional linear polarization Q/I of the scattered radiation will then be P_{21}/P_{11}, if one ignores the geometric dilution factor and the superposed contributions from continuum radiation.

The continuum introduces two effects: it dilutes the line opacity with a spectrally flat opacity, and it adds a small, spectrally flat polarization contribution. With these ingredients we can construct a very simple but still insightful model of the scattering polarization across the Na I D_2 – D_1 system, as follows:

$$(Q/I)_{\rm model}(\%) = s\ \frac{P_{21} + a_c\, b_c}{P_{11} + a_c}\,. \qquad (15)$$

While P_{21} and P_{11} are elements of the phase matrix for scattering in the sodium resonance lines, the wavelength-independent parameters a_c and b_c represent the spectrally flat continuum opacity and polarization, respectively. Parameter s is a global scaling factor that accounts for the geometric dilution effects. A similar model was introduced in Stenflo (1980) to successfully model the observed polarization across the Ca II K and H lines with the spectacular signature of quantum interference between the two total angular momentum states.

If there were no continuum opacity, Q/I would be $s\,P_{21}/P_{11}$ and look like the solid curve in Fig-

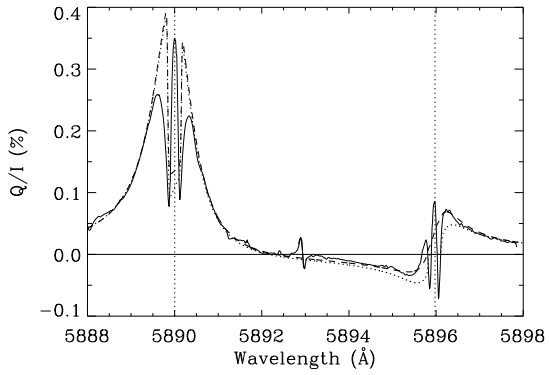

Fig. 6.— Modeling of the observed (solid curve) linear polarization Q/I across the solar Na D_2 and D_1 lines, obtained from the observations of Stenflo et al. (2000a) with the spectrograph slit 5 arcsec inside the solar limb. The dashed curve is based on the new theory, the dotted curve on the standard theory. The model uses LSA (last scattering approximation) as expressed by Equation (15). Notice in particular that the anti-symmetric behavior of the dotted model curve around the D_1 resonance gets broken by the new interference terms, which gives rise to a systematic positive polarization surplus centered around the D_1 resonance wavelength.

ure 5, only differing in the scaling factor, which has no effect on the shape of the curve. In the far wings both P_{21} and P_{11} go to zero, with the consequence that Q/I asymptotically approaches $s\,b_c$, the continuum polarization level.

The most detailed, high S/N ratio explorations of the non-magnetic scattering polarization across the Na I D_2 – D_1 system were carried out with the ZIMPOL imaging polarimeter at the NSO/Kitt Peak McMath-Pierce facility in 1998 (Stenflo et al. 2000a). The solid curve in Figure 6 shows the observed fractional Q/I polarization recorded with the spectrograph slit 5 arcsec inside the solar limb. It shows a remarkable polarization peak not only in the Doppler core of the D_2 line, but at the center of the D_1 line as well, where it was totally unexpected, because the intrinsic polarizability W_2 is zero there, even in the presence of hyperfine structure splitting (cf. Figure 4).

The dashed and dotted curves in Figure 6 are models based on Equation (15). The dotted curve represents standard scattering theory, while the dashed curve is based on the solid line of Figure 5 for P_{21}/P_{11} that was obtained with the new theory. To make the model parameters dimensionless, we normalize P_{21} and P_{11} in terms of the value of P_{11} at 5893 Å. The parameter values $a_c = 17$ and $b_c = 0.0035$ have been used for both the dashed and dotted curves, but a somewhat different global scaling factor s had to be chosen for the two curves: 0.84 for the dashed and 0.94 for the dotted one. The criterion for this choice was to make the dashed and dotted curves coincide across the D_2 line and in the far red wing of the D_1 line, at the same time as achieving an excellent fit to both the blue and red wings of the D_2 line and to the red wing of the D_1 line. It is indeed remarkable that the simple model of Equation (15) allows such a close fit.

While the D_2 fits of the dashed and dotted curves are identical, we notice in Figure 6 that the dashed curve fits the observations significantly better in the near D_1 wings, both on the blue side (where the polarization is negative) and the red side of the D_1 resonance. While the dotted curve of the standard scattering theory is anti-symmetric around the D_1 resonance, the new interference terms raise the D_1 polarization in the positive direction on both sides of the line, as already indicated by the behavior of P_{21}/P_{11} that we saw in Figure 5.

The simple LSA model of Equation (15) cannot be expected to be any good in the Doppler cores and their immediate surroundings of strong resonance lines, because these optically very thick regions are governed by intricate radiative-transfer effects, with dramatic height and wavelength variations of the anisotropy of the radiation field, and with profile-shaping effects of partial frequency redistribution (PRD). Thus it is well known that the Q/I profiles of strong resonance lines are characterized by a narrow central peak in the Doppler core, surrounded by sharp polarization minima and broader wing maxima (Rees & Saliba 1982; Holzreuter et al. 2005), exactly of the kind that we see not only in Figure 6 for the observed D_2 profile, but also for example for the Ca I 4227 Å line (Stenflo 1974; Bianda et al. 1999) and for the Ca II K line at 3933 Å (Stenflo 2003). In the case of the Na D_2 line it was explicitly demonstrated by

Fluri et al. (2003) that the Q/I triplet-type structure with the narrow core peak could indeed be explained as the result of effects in polarized radiative transfer with PRD.

While the D_1 core peak with its surrounding sharp minima looks qualitatively similar to the corresponding D_2 line core structure, it has previously not been possible to explain the centered D_1 core peak in terms of PRD effects in polarized radiative transfer. The reason is that with standard scattering theory one gets an antisymmetric shape of the P_{21}/P_{11} curve around the D_1 resonance. This has the consequence that the symmetric frequency redistribution mixes the positive contributions from the red side of the line with the equally large negative contributions from the blue side of the line, which leads to cancellation of the PRD effects. The situation changes radically with the introduction of the new interference effects, because they break the antisymmetry by adding a contribution that is positive on both sides of the line. There will be no cancellation effects when frequency redistribution acts on this symmetric component.

A good way to understand how this works is to treat the sodium phase matrix as the sum of two separate phase matrices: one representing standard theory, the other governed exclusively by the new, previously overlooked, contributions. The two phase matrices will appear in the polarized radiative transfer equation as two separate scattering source functions. While the source function that originates from standard scattering theory will not generate any PRD polarization peak because of the cancellation effects of the antisymmetric profile, the source function that represents the new contributions can serve as a source for a positive and symmetric polarization peak in the Doppler line core.

The difference between the new and the old (standard) scattering theory is only significant around the D_1 line and vanishes elsewhere. Figure 7, which represents the difference between the dashed and dotted curves in Figure 6, indicates what the main observable consequences of the new interference terms are. Since the LSA model cannot be expected to be very useful in the Doppler core, one should not assign any particular significance to the odd-looking sharp dip of the difference profile. It is an artefact of our model simplifications and should not distract from the demonstration that the new interferences contribute to a positive Q/I polarization peak that is nearly symmetric around the D_1 resonance.

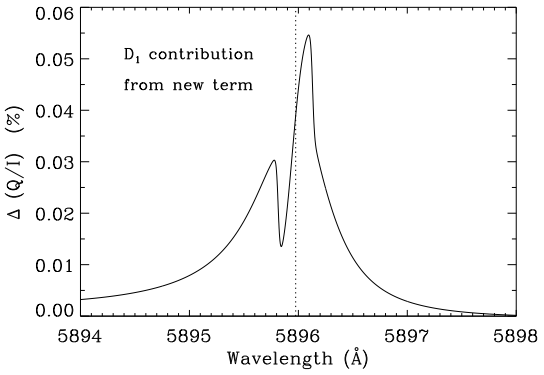

Fig. 7.— Illustration of the surplus polarization that is generated by the scattering contributions from the new term on the right-hand side of Equation (14). It represents the difference between the dashed and dotted model curves of Figure 6 and demonstrates that the new Q/I contributions are positive and nearly symmetric around the Na D_1 resonance.

This leads to the plausible conjecture that if full polarized radiative transfer with PRD were to be carried out for D_1 when the new interferences are included, then a triplet-type polarization structure of the observed kind (as shown by the solid curve in Figure 6) may emerge, because the D_2 line is structured this way, and we expect that the D_1 and D_2 lines are formed in similar ways. Only explicit radiative-transfer modeling will answer the question whether this conjecture is correct or not.

6. Application to laboratory scattering in the K D_1 line

Observational benchmarks for testing new theories require laboratory experiments, where we can explore the physics under controlled conditions. In contrast, in the solar laboratory the parameters are chosen by the Sun and are not directly known to the observer. The only published laboratory data that are relevant to the physics of the present paper were obtained a decade ago, based on an exploration of polarized scattering in the

D_1 and D_2 lines of potassium. The experiment has been described in detail by Thalmann et al. (2006, 2009). It was found that the K I D_1 line has a considerable polarization structure, which proves that it is not at all a "null line" as it has been predicted to be according to standard scattering theory. This observation has led to the conclusion that scattering theory has to be extended to include previously overlooked interferences, which occur because of fine or hyperfine structure splitting of the ground state into separate substates (Stenflo 2009, 2015a,b).

Potassium rather than sodium was chosen for the experiment, because convenient solid-state tunable lasers are available for the K I D_2 7665 Å and the K I D_1 7699 Å wavelengths. While the experiment had many degrees of freedom we will limit the discussion here to 90° scattering of linearly polarized light. The Stokes coordinate system is chosen such that the positive Stokes Q direction is defined to be perpendicular to the scattering plane. We focus our attention on two cases that will give us the profiles of the crucial P_{21} and P_{22} phase matrix elements: Scattering with the incident radiation 100 % linearly polarized perpendicular to the scattering plane ($I + Q$ radiation) and 100 % linearly polarized parallel to the scattering plane ($I - Q$ radiation). From half the sum and half the difference between these two cases the P_{21} and P_{22} matrix elements can be derived.

The monochromatic incident frequency ω' is scanned across the range where the absorption resonances of either D_1 or D_2 occur, which is done by tuning the laser (with separate laser heads for D_1 and D_2). The full Stokes vector of the scattered beam can be measured, but there is no spectral selection done in the output arm. The detector system effectively performs an integration over all the scattered frequencies ω.

The working temperature of the vapor cell is approximately 100° C, which gives a thermal Doppler width of 10.2 mÅ for potassium. The cell is filled with an argon buffer gas that prevents diffusion of the heated potassium atoms to the cooler cell windows, where they could cause opaque deposits. The collisions of the potassium atoms with the buffer gas however lead to both collisional broadening and depolarization effects, which greatly complicates the interpretation of the measurements. We therefore need to make use of a theory for partial frequency redistribution (PRD) with the collisional effects entering via different branching ratios as well as in the form of line broadening and collisional depolarization or decoherence. The problem is that such a theory only exists for the 2-level case with standard scattering. Our only option here is to make a phenomenological extension of this PRD theory to the multi-level case, and in particular define in a parametrized and heuristic way how collisions affect the new interference terms. The details of this is dealt with in Appendix C. While the presence of collisions seriously complicates the quantitative modeling of the polarization effects, the qualitative aspects, sign behavior, and orders of magnitude are not affected. We recall that standard scattering theory predicts null results for the cases that we will consider, regardless of the PRD theory used. It can therefore never be brought into any agreement with the observations.

6.1. Mueller matrix of the experiment

The temperature of the vapor cell determines the number density of potassium atoms and is chosen as a compromise: high to give sufficient scattering probability, but not too high to avoid multiple scattering effects. As the optical depth of the cell scales with the number density, the optimum compromise setting results in an effective optical depth that is smaller, but not much smaller, than unity. If we define τ as the optical depth at line center, where the intensity profile Φ_I has a maximum, then as explained in Stenflo (2015b) we find from model fitting that the measurements were done with $\tau = 0.25$ for D_1 (and therefore with $\tau = 0.50$ for D_2, due to the twice larger oscillator strength of the D_2 line). This value of τ was needed to explain the observed field strength sensitivity of the D_1 Q polarization in the case of $+Q \rightarrow Q$ scattering (incident radiation linearly polarized perpendicular to the scattering plane), because for vanishing τ the scattered Q has almost no field dependence.

The optical depth effects are so small that they may be ignored for the non-magnetic cases of scattering of linearly polarized light that we will consider here, but we include them here for completeness. They have been accounted for in the model computations. Extending the approach of Stenflo

(2015b), we express the effective Mueller matrix of the scattering experiment as

$$\boldsymbol{M}_{\rm eff}(\omega,\omega') = \boldsymbol{M}_{\rm arm}(\omega)\ \boldsymbol{R}(\omega,\omega')\ \boldsymbol{M}_{\rm arm}(\omega')\,, \tag{16}$$

where $\boldsymbol{R}(\omega,\omega')$ is the redistribution matrix in the laboratory frame, and

$$\boldsymbol{M}_{\rm arm} = e^{-\boldsymbol{\Phi}\,\tau} \tag{17}$$

is the Mueller matrix for the input or output cell arm. $\boldsymbol{\Phi}$ is the area-normalized standard Mueller absorption matrix (cf. Appendix C.3). The exponentiation of a matrix is as usual defined by its Taylor expansion.

In the experimental setup the input and output are treated in fundamentally different ways. The Mueller matrix $\boldsymbol{M}_{\rm obs}$ that is actually measured is the one that is obtained after the detector system has integrated over all the scattered frequencies:

$$\boldsymbol{M}_{\rm obs}(\omega') = \int \boldsymbol{M}_{\rm eff}(\omega,\omega')\ {\rm d}\omega\,. \tag{18}$$

This gives us all the Mueller matrix elements as functions of the incident frequency that is tuned by the laser.

6.2. Model Fitting

The phenomenologically extended PRD theory that we use for dealing with the collisional effects to model the laboratory experiment is defined in Appendix C. The free parameters of the model are the elastic collision rate Γ_E, the rate of destruction of the $2K$-multipole $D^{(K)}$, and the optical depth τ. In addition we have for the new interference terms introduced a scaling factor k_g, which physically represents an enhanced vulnerability to collisional destruction of the polarization.

The ratio $D^{(K)}/\Gamma_E$ is 0.5 in classical scattering theory (Bommier & Stenflo 1999). Although it can assume other values in quantum physics, the values do not tend to deviate that much from 0.5. Therefore we eliminate one free parameter by fixing the ratio $D^{(K)}/\Gamma_E = 0.5$.

As mentioned in the previous subsection, a non-zero value of τ is needed to explain the observed magnetic-field sensitivity of linearly polarized scattering. Modeling in Stenflo (2015b) fixed its value to $\tau = 0.25$ for K D_1 (while it is 0.5 for K D_2). Apart from contributing slightly to the line broadening it has no other significant effect on the non-magnetic scattering that we will consider here.

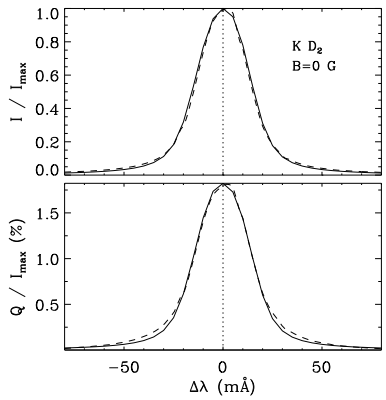

Fig. 8.— Theoretical fit (solid curves) of the Stokes I (upper panel) and Q (lower panel) profiles that have been observed in the laboratory (dashed curves) for non-magnetic 90° scattering at potassium gas with the incident radiation 100 % linearly polarized perpendicular to the scattering plane. The scale of the D_2 polarization is governed by the elastic collision rate Γ_E, which for this fit is 77 times the natural radiative Γ. With this damping and the known thermal Doppler broadening, we automatically achieve a perfect fit of the line width, without the need for any additional broadening mechanism.

We are therefore left with only two remaining free parameters, Γ_E and k_g. While k_g is significant for D_1 scattering, its effect on D_2 is completely negligible, since the D_2 polarization is governed almost exclusively by standard scattering theory. As the D_2 polarization amplitude decreases strongly and monotonically with increasing Γ_E (due to the collisional depolarization), Γ_E gets uniquely determined by fitting the observed D_2 polarization amplitude.

Figure 8 shows the nearly perfect fit between model (solid curves) and observations (dashed curves) for the case of non-magnetic D_2 scattering, when the incident radiation is linearly polarized perpendicular to the scattering plane. $\Gamma_E = 77\,\Gamma$ for this fit, where Γ is the radiative damping constant. Note that although the model only aims at reproducing the observed amplitude with the

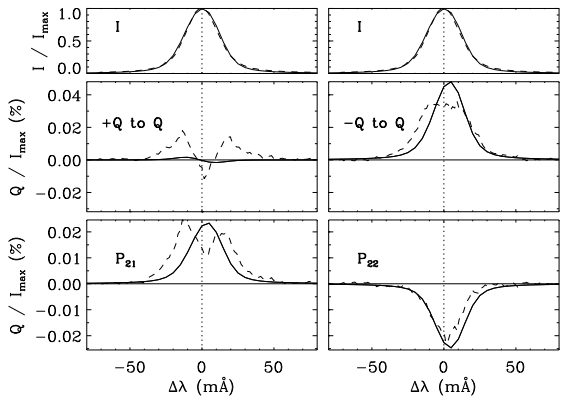

Fig. 9.— Theoretical model fits (solid curves) of laboratory K D_1 scattering data for the same model parameters as used for the K D_2 fit in Figure 8, while choosing $k_g = 0.4$ for the special depolarization parameter of the D_1 model. The experimental data, from Thalmann et al. (2006), are the same as illustrated in Figure 1, except that we have here added a correction for an assumed $I \rightarrow Q$ cross talk of 2.0×10^{-4}. This correction has however no effect on the P_{22} panel at the bottom right. The main signature of the new interference effects is the opposite signs of the P_{21} and P_{22} matrix elements, while standard theory predicts null results.

single free parameter Γ_E, the profile widths and shapes get automatically reproduced as well, without any additional assumptions or parameters. The width is determined by the thermal Doppler broadening, which is known and therefore fixed, the damping width that is dominated by Γ_E, and to some extent by τ (which was fixed by the field-sensitivity criterion for D_1). With a significantly smaller value for Γ_E we would have had to assume some additional, ad hoc broadening mechanism to achieve agreement between the profile widths of the model and the observations. With a significantly larger Γ_E no fit of the profile width would be possible at all. This demonstrates the full consistency of the parameter fit.

We can now do the D_1 model fitting with only one free parameter, k_g. The observations that we want to reproduce are the ones that have been illustrated in Figure 1, which was adapted from Thalmann et al. (2006) and represents non-magnetic scattering of linear polarization in the K D_1 line. Here we only use the results obtained with full laser power, reproduced as the dashed curves in Figure 9, because they are the same as the ones obtained with ten times less power. We have also added an instrumental $I \rightarrow Q$ cross talk correction to the experimental data, as explained below. The theoretical profiles are given by the solid curves.

The panel labeled "$+Q$ to Q" represents the measurements when the input radiation is 100 % linearly polarized perpendicular to the scattering plane, the panel labeled "$-Q$ to Q" when the input radiation is 100 % linearly polarized parallel to the scattering plane. These two panels therefore represent the combinations $P_{21} \pm P_{22}$, respectively, of the phase matrix elements, normalized to $P_{11,\max}$. Due to the large collisional depolarization $|P_{12}|$ can be neglected in comparison with P_{11}, which implies that Stokes I is represented by P_{11} alone. The observational curves in the bottom panels for P_{21} and P_{22} are then obtained by taking half the sum and half the difference of the middle panels.

Like for D_2 the Stokes I profile width depends significantly on the collisional damping width Γ_E. The nearly perfect model fit to the D_1 Stokes I profile in the top panels validates the self-consistency of the Γ_E parameter as determined from the D_2 observations.

In contrast to the observations, the theoretical model calculations give the phase matrix elements of the bottom panels directly, from which the $\pm Q$ to Q versions of the middle panels are then derived. Comparison between the theoretical and observational curves shows qualitative agreement as concerns the relative signs of the phase matrix elements and the order of magnitude of their amplitudes, but the agreement is significantly better for the P_{22} diagram, which is unaffected by $I \rightarrow Q$ instrumental cross talk, than for the other three diagrams of the middle and bottom panels of Figure 1, when they are uncorrected for the cross talk. This leads us to suspect that some of the discrepancies have to do with such cross talk.

Because Stokes I is so much larger than the other Stokes parameters, the instrumental polarization is dominated by the $I \rightarrow Q$ cross talk, which may arise from stresses in the exit window of the vapor cell. It can be accounted for in the model by adding a fraction f of the I profile of the

top panels to the measured Q of the middle panels. This I fraction then also gets added to the bottom left panel for P_{21}, because it is obtained as the average of the two middle panels, but it gets subtracted away in the bottom right panel for P_{22}, which is formed from half the difference between the middle panels. We find that the application of a cross talk fraction $f = 2.0 \times 10^{-4}$ significantly improves the fit. This (quite small) cross talk correction has therefore been applied to the experimental data in Figure 9.

Besides the cross talk correction we find that the model amplitudes would be too high by a factor between 2 and 3 unless we make use of the free scaling parameter k_g. A value of $k_g = 0.4$ has therefore been used in Figure 9 to optimize the fit. It may be interpreted as an enhanced vulnerability to collisional depolarization as compared with the depolarization that is expected from the standard branching ratios in PRD theory.

The main property that is well expressed by our model is the observed symmetry breaking between the P_{21} and P_{22} phase matrix elements. According to standard scattering theory they should both be zero. In contrast, the observations show P_{22} to be negative, P_{21} to be positive.

Nevertheless there still remain important modeling problems. The profile shapes are not fully reproduced even after introducing the correction for $I \rightarrow Q$ cross talk, and the k_g scaling represents an extra free parameter that cannot be derived from the theory. While we still do not have a full understanding of D_1 scattering physics, much of the present modeling complications have to do with the circumstance that the scattering takes place in a collision-dominated regime. A heuristic extension of phenomenological polarized frequency redistribution theory cannot be expected to properly describe the detailed redistribution physics in this regime in the presence of new, previously unexplored, interference effects. We need a laboratory experiment for the collision-free regime to eliminate such irrelevant complications, so that we may more directly address the fundamental issues concerning the quantum scattering of light.

One objection that has been raised about our experimental D_1 results is that there could be collisional transfer of atomic polarization from the upper state of D_1 to that of D_2, which is then radiated away in the D_2 line. Since we do not have spectral discrimination in the output arm of the experiment, we cannot distinguish such D_2 photons from those that are scattered within the D_1 transition. However, this objection is unfounded, because the velocity distribution of the buffer gas colliders is thermal and therefore isotropic. Without any preferred spatial orientation the collisions are incapable of transferring any polarization, even if significant D_1 to D_2 collisional transfer would take place (which is also highly questionable). Although we therefore believe that collisions with the buffer gas can be completely ruled out as a possible source of polarization, this kind of debates would be unnecessary for an experiment in the collision-free domain.

7. Outlook

Scattering of light is a cornerstone process in physics that needs to be deeply understood in all of its aspects. Although laboratory experiments on polarized scattering was a hot topic in the early days of quantum mechanics, because they allowed explicit demonstration of the fundamental concept of coherent superposition of atomic states in various situations, the scientific community turned to other topics around 1935, apparently because it was felt that the experimental possibilities had been exhausted with the technology that was available at that time. This technology was incredibly crude by today's standards. Using tunable lasers as light sources, electro-optical polarization modulators, and photoelectric detectors we can now do orders of magnitude better and explore parameter domains that were entirely inaccessible at that time.

The motivation to return to this topic after it had for many decades been considered to be sufficiently understood, came from observations of polarization anomalies in the Sun's spectrum. For the resolution of the D_1 enigma one needed a laboratory experiment under controlled conditions. Such an experiment was carried out a decade ago for polarized scattering at potassium vapor. Although it unequivocally revealed that available scattering theory is indeed incomplete, the general reaction of the community was one of unsubstantiated disbelief. The feeling was that the theory for the scattering of light has been used for so many decades that it cannot be wrong and does not

need to be tested. Therefore there must be something wrong with the experiment (for instance that there must be some special effects when using laser light, collisions may transfer polarization to the D_2 line, or there are some unidentified instrumental problems). Instead of trying to examine if any of these various objections could have some merit, the reaction to the "inconvenient evidence" was rather to look away and continue with "business as usual".

This behavior brings to mind the wise words of the eminent Austrian-British science philosopher Karl Popper in a quote from 1957: "If we are uncritical we shall always find what we want: we shall look for, and find confirmations, and we shall look away from, and not see, whatever might be dangerous to our pet theories." For Popper the most important element for progress in experimental science is the falsification of theories, and not their verification. In the context of the D_1 problem it is the falsification of standard scattering theory that is the by far most important aspect, while the degree of success of the new modeling attempts is secondary. After the falsification aspect has now been taken care of, a next generation of laboratory experiments will be needed to guide the development of an extended scattering theory that can satisfy all observational constraints in parameter domains where it has not been experimentally tested before.

7.1. Next steps

In the solar case the application that we have done in the present paper to compare the extended scattering theory with the observations is incomplete, because proper modeling of the solar line profiles requires radiative transfer with partial frequency redistribution. Fortunately the sodium D_1 line core is formed at heights in the solar atmosphere, where collisional effects are rather unimportant, which justifies the collision-free application of the theory. As collisional branching ratios are then not needed, the redistribution matrix $\boldsymbol{R}$ in Equation (C8) is given exclusively by matrix $\boldsymbol{R}_{\rm II}$, which greatly simplifies the radiative transfer problem. We may expect that redistribution acting on the nearly symmetric profile of Figure 7 for the surplus D_1 polarization, which is generated by the new interference effects, will lead to a final profile shape that is qualitatively similar to that of the D_2 profile, as needed for agreement with the observed D_1 profile shape. This conjecture needs to be tested. Still the solar laboratory is inferior to terrestrial laboratories for the purpose of unambiguous tests of theories, because we have no control over the physical parameters on the Sun.

The laboratory experiment done so far has for convenience used a potassium vapor cell with an argon buffer gas, which led to undesired high collision rates causing line broadening and depolarization. It then became unavoidable to do modeling in the collision-dominated domain with heuristically extended PRD physics. For the next generation of scattering experiments the first priority should be to avoid such complications in order to do "clean" tests of the various aspects of scattering physics. The experiment should therefore be done in the collision-free regime without the use of any buffer gas. Once this regime has been sufficiently explored, including the effects of imposed external magnetic fields, one would have a foundation that could later be extended by exploring collisional physics and PRD in the laboratory. The various applications of scattering theory, e.g. in astrophysics, need to be based on a solid foundation that should always be validated in the laboratory, as we have learnt from the example of the D_1 enigma.

The next generation of experiments with polarized scattering are being considered in collaboration with INLN (Institut Non-Lineaire de Nice) in France, where they have facilities and experience for doing various kinds of atomic-physics experiments with rubidium vapor without the use of any buffer gas (cf. Baudouin et al. 2014; Guerin et al. 2016). It is possible to do the experiment with the natural mixture of the two main Rb isotopes 85 and 87 or with each of the isotopes separately. External magnetic fields of various strengths and orientations may be imposed, and the rubidium may be supercooled to microkelvin temperatures if desired (to eliminate all Doppler broadening). This would open the door to a vast parameter space to achieve in-depth clarification of the various aspects of scattering theory.

In anticipation of the future laboratory experiments we apply the present version of our extended scattering theory to make a definite prediction in Figures 10 and 11 of what we may expect to find in the case of non-magnetic, collision-free 90°

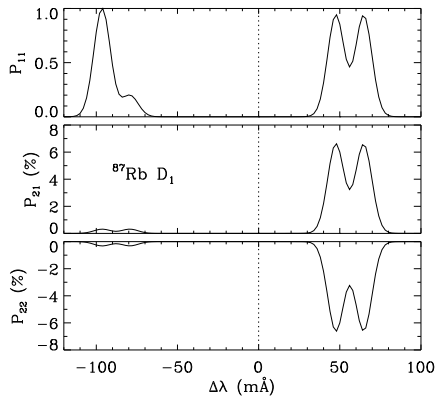

Fig. 10.— Predicted phase matrix elements P_{11}, P_{21}, and P_{22}, given in units of $P_{11,\,\mathrm{max}}$, for 90° D_1 scattering at rubidium isotope 87 (which has nuclear spin 3/2). Note the perfect anti-symmetry between P_{21} and P_{22}. The reference wavelength for the relative wavelength scale is 7947.6712 Å.

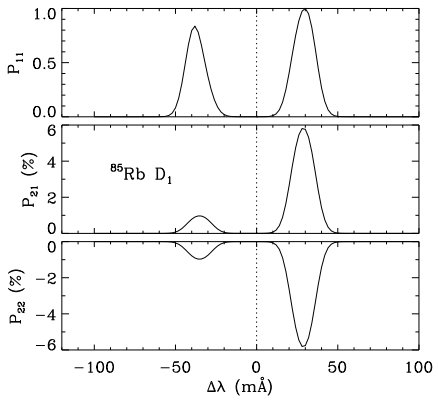

Fig. 11.— Same as Figure 10 but for D_1 scattering at rubidium isotope 85 (which has nuclear spin 5/2).The reference wavelength for the relative wavelength scale is the same as in Figure 10.

scattering at rubidium vapor. The prediction is illustrated for the phase matrix elements P_{11} (normalized intensity) and P_{21} and P_{22}, which govern the linear polarization and are the matrix elements that are relevant to the solar D_1 enigma and the K D_1 experimental results that were illustrated in Figure 9. As before, the Stokes coordinate system is defined such that the positive Stokes Q direction is perpendicular to the scattering plane.

The natural isotope composition of rubidium is 72.2 % of isotope 85 with nuclear spin 5/2, and 27.8 % of isotope 87 with nuclear spin 3/2. The isotopes may be purified to be scattered at separately, but if the experiment is done for the natural isotope mixture, then the predictions of Figures 10 and 11 should be weighted together in proportion to the corresponding relative abundances after the relative isotope shift has been accounted for. The isotope shift of +1.46 mÅ of isotope 85 relative to isotope 87 has already been applied to Figure 11 (although it is too small to be visible in the plot), so that both relative wavelength scales in fact refer to the same reference wavelength, 7947.6712 Å.

Rb isotope 87 has the same nuclear spin as sodium and potassium, but the hyperfine structure splitting (HFS) is approximately 16 times larger for Rb than for potassium. Therefore the Rb HFS components are so widely separated that there is hardly any overlap between them. In the case of the K lab experiment we had in addition collisional line broadening by a factor of 77, which greatly contributed to the overlap of the profiles from the different HFS components. Such overlap does not occur in the collision-free Rb case.

We notice in both of Figures 10 and 11 the perfect anti-symmetry between the P_{21} and P_{22} matrix elements. This predicted anti-symmetry is a special signature of the new interference terms in our present version of the extended theory. It should be stressed, however, that any observed non-zero features in the spectra of P_{21} and P_{22} would falsify standard scattering theory, which predicts both of them to be zero for all wavelengths. The laboratory experiments are needed to guide us in the difficult process of formulating a theory that is able to satisfy all observational constraints.

For the modeling of the scattering polarization I have greatly profited from an IDL code provided to me by Svetlana Berdyugina and Dominique Fluri, with which one can conveniently calculate the atomic level structure and transition amplitudes in the Paschen-Back regime for the sodium and potassium D_1 – D_2 systems, and from an extension of this code by K. Sowmya to the rubidium isotopes 85 and 87.

REFERENCES

Baudouin, Q., Guerin, W., & Kaiser, R. 2014, Annual Review of Cold Atoms and Molecules, 2, 251

Belluzzi, L., Trujillo Bueno, J., & Landi Degl'Innocenti, E. 2015, ApJ, 814, 116

Bianda, M., Stenflo, J. O., & Solanki, S. K. 1999, A&A, 350, 1060

Bommier, V. 1997a, A&A, 328, 706

Bommier, V. 1997b, A&A, 328, 726

Bommier, V. & Stenflo, J. O. 1999, A&A, 350, 327

Cohen-Tannoudji, C. & Reynaud, S. 1977, J. Phys. B: Atom. Molec. Phys., 10, 345

Dirac, P. A. M. 1947, The principles of quantum mechanics — Third Edition (Oxford: Clarendon Press)

Faurobert-Scholl, M., Feautrier, N., Machefert, F., Petrovay, K., & Spielfiedel, A. 1995, A&A, 298, 289

Feller, A. J. 2008, Diss. ETH No. 17333: Instrument Systems for Imaging Spectro-Polarimetry (Göttingen: Cuivillier Verlag)

Fluri, D. M., Holzreuter, R., Klement, J., & Stenflo, J. O. 2003, in Astronomical Society of the Pacific Conference Series, Vol. 307, Solar Polarization 3, ed. J. Trujillo-Bueno & J. Sanchez Almeida, 263

Guerin, W., Araújo, M. O., & Kaiser, R. 2016, Physical Review Letters, 116, 083601

Holzreuter, R., Fluri, D. M., & Stenflo, J. O. 2005, A&A, 434, 713

Kramers, H. A. & Heisenberg, W. 1925, Z. Phys., 31, 681

Landi Degl'Innocenti, E. 1998, Nature, 392, 256

Landi Degl'Innocenti, E. & Landolfi, M. 2004, Astrophysics and Space Science Library, Vol. 307, Polarization in Spectral Lines (Kluwer)

Loudon, R. 2000, The Quantum Theory of Light — Third Edition (Oxford Univ. Press)

Omont, A., Smith, E. W., & Cooper, J. 1972, ApJ, 175, 185

Omont, A., Smith, E. W., & Cooper, J. 1973, ApJ, 182, 283

Rees, D. E. & Saliba, G. J. 1982, A&A, 115, 1

Sampoorna, M., Nagendra, K. N., & Stenflo, J. O. 2007, ApJ, 670, 1485

Spielfiedel, A., Feautrier, N., Chambaud, G., & Lévy, B. 1991, J. Phys. B.: At. Mol. Opt. Phys., 24, 4711

Steck, D. A. 2010, Sodium D Line Data, revision 2.1.4, 23 December 2010 (available online at http://steck.us/alkalidata)

Stenflo, J. O. 1974, Sol. Phys., 37, 31

Stenflo, J. O. 1980, A&A, 84, 68

Stenflo, J. O. 1994, Solar Magnetic Fields — Polarized Radiation Diagnostics. (Kluwer)

Stenflo, J. O. 1998, A&A, 338, 301

Stenflo, J. O. 2009, in Astronomical Society of the Pacific Conference Series, Vol. 405, Solar Polarization 5, ed. S. V. Berdyugina, K. N. Nagendra, & R. Ramelli, 3–16

Stenflo, J. O. 2011, in Astronomical Society of the Pacific Conference Series, Vol. 437, Astronomical Society of the Pacific Conference Series, ed. J. R. Kuhn, D. M. Harrington, H. Lin, S. V. Berdyugina, J. Trujillo-Bueno, S. L. Keil, & T. Rimmele, 3–17

Stenflo, J. O. 2015a, in IAU Symposium, Vol. 305, Polarimetry, ed. K. N. Nagendra, S. Bagnulo, R. Centeno, & M. Jesús Martínez González, 136–145

Stenflo, J. O. 2015b, ApJ, 801, 70

Stenflo, J. O., Gandorfer, A., & Keller, C. U. 2000a, A&A, 355, 781

Stenflo, J. O. & Keller, C. U. 1996, Nature, 382, 588

Stenflo, J. O. & Keller, C. U. 1997, A&A, 321, 927

Stenflo, J. O., Keller, C. U., & Gandorfer, A. 2000b, A&A, 355, 789

Thalmann, C., Stenflo, J. O., Feller, A., & Cacciani, A. 2006, in Astronomical Society of the Pacific Conference Series, Vol. 358, Solar Polarization 4, ed. R. Casini & B. W. Lites, 323

Thalmann, C., Stenflo, J. O., Feller, A., & Cacciani, A. 2009, in Astronomical Society of the Pacific Conference Series, Vol. 405, Solar Polarization 5: In Honor of Jan Stenflo, ed. S. V. Berdyugina, K. N. Nagendra, & R. Ramelli, 113

This 2-column preprint was prepared with the AAS LaTeX macros v5.2.

A. Rabi frequency for the laboratory experiment on potassium scattering

The Rabi frequency ω_R for a given transition between m states i and j is

$$\omega_R = \frac{\boldsymbol{d}_{ij} \cdot \boldsymbol{E}_0}{\hbar} \,, \tag{A1}$$

where $\boldsymbol{d}_{ij}$ is the electric dipole moment of the transition, and $\boldsymbol{E}_0$ is the amplitude of the electric vector of the external radiation field. $\boldsymbol{d}_{ij} \cdot \boldsymbol{E}_0$ represents the interaction energy between the atom and the radiation field.

Let $\mathcal{P}_{\rm laser}$ be the power of the laser beam, which is expanded to fill the effective cross section $\sigma_{\rm cell}$ of the vapor cell where the scattering takes place. Then

$$\frac{\mathcal{P}_{\rm laser}}{c\ \sigma_{\rm cell}} = \epsilon_0 |E_{0q}|^2 \,, \tag{A2}$$

where the left-hand side represents the radiative energy density of the laser beam, and E_{0q} is the polarization component of the 100 % polarized beam, which induces the ij atomic transition. The corresponding component of the dipole moment that is radiatively excited can be expressed in terms of the Einstein A_{ji} coefficient (cf. Loudon 2000):

$$d_q = (3\pi\epsilon_0\, c^3\, \hbar\, A_{ji}/\omega_0^3\,)^{1/2} \,. \tag{A3}$$

Combining Equations (A1) – (A3) we find

$$\omega_R = \Big(\frac{3}{4\pi^2}\ \frac{\mathcal{P}_{\rm laser}\ \lambda^3}{c\,\hbar\,\sigma_{\rm cell}}\ A_{ji} \Big)^{1/2} \,. \tag{A4}$$

With the maximum laser power 15 mW for $\mathcal{P}_{\rm laser}$, 7698.97 Å for the K D_1 resonance, 1 cm^2 for the cell cross section $\sigma_{\rm cell}$, and $3.82 \times 10^7\,{\rm s}^{-1}$ for the A_{ji} coefficient, we find $\omega_R \approx 7.9 \times 10^7\,{\rm s}^{-1}$, approximately 2.1 times larger than A_{ji}.

Converted to wavelength units, the radiative Γ, taken as A_{ji}, is 0.12 mÅ, while the Rabi frequency corresponds to 0.25 mÅ. Model fitting of the K D_2 line gives an elastic collision rate $\Gamma_E \approx 77\Gamma$. The total damping width $\Gamma + \Gamma_E$ then corresponds to 9.4 mÅ, which is comparable to the thermal Doppler width (10.3 mÅ) and 38 times larger than the corresponding Rabi frequency.

To rule out a possible dependence of the scattering polarization on the Rabi frequency we have compared results obtained with full laser power and with the power reduced by a factor of ten. As documented in Figure 1 one cannot discern any significant difference between the corresponding polarization profiles, which verifies that the relatively high radiation energy density of the laser beam does not affect the polarization phenomena that we are exploring.

B. Expression for the transition matrix elements

The matrix elements that define the atomic transitions in the Kramers-Heisenberg formulation can be expressed algebraically with the help of the Wigner-Eckart theorem and expansions of the reduced matrix elements $\langle F \,||\, e\,\hat{\boldsymbol{r}} \,||F'\rangle$ and $\langle J \,||\, e\,\hat{\boldsymbol{r}} \,||J'\rangle$, using well-known formulae given for instance in Stenflo (1994) and Steck (2010). The resulting expression for the non-magnetic case is

$$\begin{aligned} \langle F\, m|\, e\,\hat{r}_q |F' m'\rangle \;=\; & \langle L \,||\, e\,\hat{\boldsymbol{r}} \,||L'\rangle\, (-1)^{L+S+I+1} \sqrt{2L+1} \\ & (-1)^{J+J'+2F'+m} \sqrt{(2J+1)(2J'+1)(2F+1)(2F'+1)} \\ & \begin{Bmatrix} L & L' & 1 \\ J' & J & S \end{Bmatrix} \begin{Bmatrix} J & J' & 1 \\ F' & F & I \end{Bmatrix} \begin{pmatrix} F' & 1 & F \\ m' & q & -m \end{pmatrix} . \end{aligned} \tag{B1}$$

Since L, L', S, and I are the same for all the members of a given supermultiplet, the three factors in the first row of the above equation are of no consequence for the polarization, because they divide out when forming the phase matrix (which is usually normalized to the maximum value of P_{11}). However, it is essential that all the remaining factors are included correctly. If they are not, the Principle of Spectroscopic Stability (PSS) will not be satisfied for all supermultiplets (all combinations of electronic and nuclear spins S and I). PSS is therefore a powerful tool to verify the correctness of the expressions and to reveal possible bugs in the computer algorithms. In the present paper we have applied it to verify that it is obeyed for all $L = 0 \rightarrow 1 \rightarrow 0$ scattering transitions for any combination of S (which defines the set of J quantum numbers) and I (which defines the set of F quantum numbers).

C. PRD and Collisional Branching Ratios

Collisions are generally regarded as discrete events in the impact approximation, but a consistent quantum-mechanical treatment is extremely complex with implicit approximations. Moreover, the theory has not been sufficiently tested in the laboratory. Most of the expressions used today in astrophysical contexts are based on the early work of Omont et al. (1972, 1973), developed into the currently used form in particular by Bommier (1997a,b). Here we will summarize the way in which collisions are currently believed to affect the scattering matrix.

Collisions change the scattering matrix in two main ways: (1) They govern the relation between the incident and scattered frequencies ω' and ω (frequency redistribution), and (2) they change the polarization of the scattered radiation. The effects of frequency redistribution and collisional depolarization are coupled to each other, but a PRD theory that describes this exists only for the 2-level standard scattering case. We therefore need to make a phenomenological extension of PRD for standard scattering theory to the multi-level case, and in addition introduce some reasonable way to do the calculations for the new scattering terms. In standard PRD theory the net effect of collisions is that each term in Equation (4) for the coherency matrix (or correspondingly each term of the Mueller matrix) can be described as a sum of two main terms, one that represents frequency coherence (which we refer to as FC and which implies that $\omega' = \omega$ in the atomic rest frame), while the other term represents complete frequency redistribution (which we refer to as CRD). The relative contribution of each is governed by a branching ratio, which we denote A for FC and B for CRD. The weighted combination of FC and CRD describes the full effect of the collisions and is referred to as PRD (partial frequency redistribution). We also have to properly attach decoherence factors due to interferences between the scattering amplitudes.

In the following subsection we will outline how this standard PRD theory can be phenomenologically extended to multi-level scattering. For non-standard scattering with the new interferences as defined by the second term on the right-hand side of Equation (14) we need to introduce some further modifications of standard PRD theory to allow us to include collisional effects in a way that is well defined for modeling purposes. This heuristic extension of PRD theory is dealt with in Subsection C.2.

C.1. Phenomenological extension of PRD for standard scattering theory

Let us by symbol $\mathcal{P}_{\rm standard}(\omega,\omega')$ denote the PRD expression for the frequency-dependent parts of the bilinear products in Equation (4) for a given combination a, a', b, b', f, f' of initial, intermediate, and final states in standard scattering theory. Then

$$\mathcal{P}_{\rm standard}(\omega,\omega') = \tfrac{1}{2}[\Phi_{\,b-a}(\omega') + \Phi^*_{b'-a}(\omega')]\cos\beta_e\, e^{i\beta_e} \left[\, A\,\delta(\omega-\omega') \,+\, B^{(K)}\,\tfrac{1}{2}[\Phi_{\,b-f}(\omega) \,+\, \Phi^*_{b'-f}(\omega)]\cos\alpha_e\, e^{i\alpha_e}\right]. \tag{C1}$$

Let Γ, Γ_I, and Γ_E be the damping constants of radiation, inelastic collisions, and elastic collisions, respectively. Then the profile functions Φ are given by Equation (2) if we do the replacement

$$\gamma = \Gamma + \Gamma_I + \Gamma_E\,. \tag{C2}$$

Index e of the decoherence angles β_e and α_e indicate that the decoherence originates exclusively from level splitting of the excited state. β_e, which relates to the absorption process, is defined by

$$\tan\beta_e = \frac{\omega_{b'b}}{\Gamma + \Gamma_I + \Gamma_E}\,, \tag{C3}$$

while α_e that relates to the emission process is defined by

$$\tan\alpha_e = \frac{\omega_{b'b}}{\Gamma + \Gamma_I + D^{(K)}}\,, \tag{C4}$$

where $D^{(K)}$ represents the destruction rate of the $2K$-multipole (the atomic polarization) when $K = 1$ or 2.

Comparison of Equations (C3) and (C4) shows that there is a fundamental difference between the absorption and emission processes (in contrast to the collisionless case), because the collisional effects enter differently in the two cases: as Γ_E and as $D^{(K)}$, respectively. This implies that the collisions manage to break the symmetry with respect to time reversal, although it remains rather obscure how they actually do it.

The branching ratios are

$$A = \frac{\Gamma}{\Gamma + \Gamma_I + \Gamma_E} \tag{C5}$$

and

$$B^{(K)} = A\ \frac{\Gamma_E - D^{(K)}}{\Gamma + \Gamma_I + D^{(K)}}\,. \tag{C6}$$

If there were symmetry between the absorption and emission processes, then $B^{(K)}$ would be exactly zero, and all scattering would be frequency coherent.

The assignment of different combinations of dipole transitions to different values of K is a technical issue that we will not go into here but only refer to the treatment in Sampoorna et al. (2007). Both classical and quantum collision theory suggest that $D^{(K)}$ should usually be of order $\Gamma_E/2$ for both $K = 1$ or 2 (Bommier & Stenflo 1999; Spielfiedel et al. 1991; Faurobert-Scholl et al. 1995), although the value depends on the atomic structure and it is even questionable to what extent the parametrization of the collisional effects in terms of the two parameters $D^{(1)}$ and $D^{(2)}$ represents a good approximation.

From Equation (C6) we see that $B^{(K)} \approx A$ for large collision rates (except in the unlikely special case when $D^{(K)} \approx \Gamma_E$), while $B^{(K)} \approx 0$ when $\Gamma_E \ll \Gamma + \Gamma_I$.

$K = 0$ represents the isotropic case without atomic or scattering polarization. Since $D^{(0)} = 0$, and since we may safely assume that $\Gamma_I \ll \Gamma_E$, Equation (C6) gives

$$B^{(0)} \approx \frac{\Gamma}{\Gamma + \Gamma_I}\,(1 - A)\,. \tag{C7}$$

This represents the case of collisionally induced isotropic, unpolarized scattering, when the collisions have erased all atomic "memory" of the excitation event, so that there is no phase or directional relations between absorption and emission processes. It will be clarified more in Section C.3 under the name *incoherent scattering*.

In terms of the Mueller scattering matrix $\boldsymbol{M}$, $K = 0$ corresponds to the isotropic component M_{11}, while all the remaining parts of $\boldsymbol{M}$ relate to either $K = 1$ or 2.

What we usually refer to as *redistribution matrices* $\boldsymbol{R}$ are Mueller matrices that are formed from the coherency matrix $\boldsymbol{W}$ after summing up the contributions from all the index combinations of a, a', b, b', f, f', making use of Equation (C1). In general one also needs to apply standard Doppler redistribution integrals to transform from the atomic rest frame to the observer's coordinate system if one wants to get the correct spectral distribution of the scattered radiation. In the special case of our laboratory scattering experiment, however, the detector system effectively integrates over all the scattered frequencies. Then it is sufficient

to do gaussian Doppler broadening for the incident frequencies over which the laser tuning is done, while ignoring how the frequencies get redistributed by the scattering process.

As in Equation (C1) $\boldsymbol{R}$ can be decomposed in a frequency coherent and a complete redistribution part, for which the respective notations $\boldsymbol{R}_{\rm II}$ and $\boldsymbol{R}_{\rm III}$ have been used in the literature. Thus we may write

$$\boldsymbol{R} = A\,\boldsymbol{R}_{\rm II} + \sum_{K=1}^{2} B^{(K)}\,\boldsymbol{R}_{\rm III}^{(K)} + \frac{\Gamma}{\Gamma+\Gamma_I}\,(1-A)\,\boldsymbol{R}_{\rm ic}\,, \tag{C8}$$

where we for convenience have introduced the notation $\boldsymbol{R}_{\rm ic}$ to represent the isotropic part $\boldsymbol{R}_{\rm III}^{(0)}$ (using index "ic" to indicate that this matrix represents incoherent scattering).

The normalization condition for $\boldsymbol{R}$ is

$$\int \frac{{\rm d}\Omega'}{4\pi} \int \frac{{\rm d}\Omega}{4\pi} \int {\rm d}\omega' \int {\rm d}\omega\ \mathbf{1}^T \boldsymbol{R}\,\mathbf{1} = 1\,, \tag{C9}$$

where

$$\mathbf{1}^T \boldsymbol{R}\,\mathbf{1} = R_{11}\,. \tag{C10}$$

R_{11} is the first element of matrix $\boldsymbol{R}$, while $\mathbf{1}$ is a 4-vector that has unity in its first position while the rest is zero. Upper index T means transposition. The angular averaging is made over all incident and scattered directions, the frequency integrations over all incident and scattered frequencies.

C.2. Heuristic extension of PRD for the new scattering terms

In analogy with Equation (C1) we let symbol $\mathcal{P}_{\rm new}(\omega,\omega')$ denote the PRD expression for the frequency-dependent parts of the bilinear products in Equation (4) that relate to the new scattering contributions in the extended theory. Since the new terms obey the special symmetry that the initial and final substates are identical ($a = f$ and $a' = f'$), there are reasons to assume full symmetry (time reversal symmetry) between the absorption and emission legs of the scattering transition. In this case the CRD branching ratio $B^{(K)}$ vanishes, and only the frequency coherent term with collisional depolarization factor A remains. These considerations lead us to the following expression:

$$\mathcal{P}_{\rm new}(\omega,\omega') = \tfrac{1}{2}[\Phi_{\,b-a}(\omega') + \Phi^*_{b-a'}(\omega')]\,k_g\,\cos^2\beta_g\,e^{2i\,\beta_g}\ A\,\delta(\omega-\omega')\,. \tag{C11}$$

While A is given by Equation (C5), the decoherenc angle β_g is defined by Equation (12) if we let γ be given by Equation (C2). Furthermore, for reasons explained in detail in Section 4.4, we need to apply the decoherence factor twice to the new interference terms, in contrast to standard scattering theory. This is why the decoherence factor appears in squared form in Equation (C11),

This expression leads to qualitatively good agreement with the laboratory results for scattering of linear polarization at potassium gas, but the predicted amplitudes of phase matrix elements P_{21} and P_{22} are larger than the observed ones by a factor of 2-3. For this reason we have in Equation (C11) introduced an ad hoc scaling factor k_g, to be used as a free parameter in the model fitting. The best fits are obtained with $k_g \approx 0.4$.

Physically a scaling factor k_g that is less than unity implies that the new interference terms, which arise from the splittings of the ground states and which are the only source of the polarization effects that are observed for K D_1 scattering, are more vulnerable to collisional destruction than accounted for by the standard collisional depolarization factor A. The simplest way to parametrize this enhanced collisional vulnerability is in terms of a single scale factor.

C.3. Incoherent Scattering

The incoherent scattering matrix $\boldsymbol{R}_{\rm ic}$ represents the case when collisions have erased the atomic polarization or "memory" of the excitation process, making the emission process unrelated to the absorption process.

The expression for the normalized incoherent scattering matrix is (cf. Stenflo 1994, p. 80)

$$\boldsymbol{R}_{\rm ic} = [\,\boldsymbol{\Phi}(\omega)\,\mathbf{1}]\,[\mathbf{1}^T\,\boldsymbol{\Phi}(\omega')]\,, \tag{C12}$$

where $\boldsymbol{\Phi}$ here represents the 4×4 Zeeman Mueller absorption matrix without anomalous dispersion. It is normalized such that integration of its first element, Φ_I, over all frequencies is unity. In more explicit form $\boldsymbol{R}_{\rm ic}$ becomes

$$\boldsymbol{R}_{\rm ic} = \begin{pmatrix} \Phi_I\Phi'_I & \Phi_I\Phi'_Q & \Phi_I\Phi'_U & \Phi_I\Phi'_V \\ \Phi_Q\Phi'_I & \Phi_Q\Phi'_Q & \Phi_Q\Phi'_U & \Phi_Q\Phi'_V \\ \Phi_U\Phi'_I & \Phi_U\Phi'_Q & \Phi_U\Phi'_U & \Phi_U\Phi'_V \\ \Phi_V\Phi'_I & \Phi_V\Phi'_Q & \Phi_V\Phi'_U & \Phi_V\Phi'_V \end{pmatrix}\,, \tag{C13}$$

where the primed functions Φ' relate to the incident frequency ω', while the unprimed Φ relate to the scattered frequency ω.

The explicit expressions for the functions $\Phi_{I,Q,U,V}$ are

$$\begin{aligned} \Phi_I &= \Phi_\Delta \sin^2\gamma + \tfrac{1}{2}(\phi_+ + \phi_-)\,, \\ \Phi_Q &= \Phi_\Delta \sin^2\gamma\,\cos 2\chi\,, \\ \Phi_U &= \Phi_\Delta \sin^2\gamma\,\sin 2\chi\,, \\ \Phi_V &= \tfrac{1}{2}(\phi_+ - \phi_-)\cos\gamma\,, \\ \Phi_\Delta &= \tfrac{1}{2}[\,\phi_0 - \tfrac{1}{2}(\phi_+ + \phi_-)\,]\,. \end{aligned} \tag{C14}$$

The ϕ_q profile functions in Equation (C14) are obtained by summing over the real part of the profile functions of all transitions for which lower level m minus upper level m equals q, then weight these functions with the respective transition probabilities (squares of the respective matrix elements), and finally do Doppler broadening and area normalization.